Vol. 16(1), pp. 37-70, January 2022
DOI: 10.5897/AJEST2021.3065
Article Number: AD6D22D68508
ISSN: 1996-0786

http://www.academicjournals.org/AJEST

ACADEMIC JOURNALS
expand your knowledge

African Journal of Environmental Science and Technology

Full Length Research Paper

Isotherms, kinetic and thermodynamic studies of methylene blue adsorption on chitosan flakes derived from African giant snail shell

Olaosebikan Abidoye Olafadehan[1*], Victor Ehigimetor Bello[1], Kehinde Olawale Amoo[2] and Adebukola Morufat Bello[1]

[1]Department of Chemical and Petroleum Engineering, University of Lagos, Akoka-Yaba, Lagos 101017, Nigeria.
[2]Department of Chemical Engineering, Lagos State University, Epe, Lagos State, Nigeria.

Received 6 September, 2021; Accepted 7 January, 2022

In the present study, modeling of 19 adsorption isotherms, 8 kinetic models and thermodynamics of methylene blue (MB) adsorption on chitosan flakes synthesized using *Archachatina marginata* shell wastes was investigated in a batch mode. The operational parameters' effects on the MB adsorption were studied. The model parameters were statistically analyzed using 10 error functions. The choices of the best fitted adsorption and kinetic models were based on the comparison of the sum of normalized error (SNE) and two statistical tools of information-based criteria. The 5-p Fritz-Schlüender isotherm best fitted the experimental adsorption data of MB on chitosan flakes based on SNE whereby maximum adsorption capacity, q_{max}, of 143.6660 mg/g was obtained. The adsorption rate of MB on chitosan flakes was kinetically described by pseudo second-order model at all initial concentrations of MB investigated, with film diffusion being the rate-controlling step and the adsorption process chemisorption-influenced. The calculated thermodynamic parameters, ΔH^0 = 4.23 kJ/mol, ΔS^0 = 0.4563 kJ/(mol K), negative ΔG^0 values revealed that the adsorption of MB onto chitosan flakes was physical, endothermic, spontaneous, energetically favorable and exergonic. The reaction mechanism of the adsorption of MB onto chitosan flakes was proposed taking cognizance of the electrostatic force of attraction between the negatively charged surface of the chitosan (biosorbent) and the positively charged MB.

Key words: chitosan, dye adsorption, isotherm, kinetics, thermodynamics, information-based criteria.

INTRODUCTION

The use of dyes in dyeing and printing processes is quite enormous, which is evident in many industries globally (Afroze et al., 2015). The perennial discharges of wastewater containing dyes from textile, dyeing, pharmaceutical, food, cosmetics and healthcare, paper and leather industries, amongst others, into the water

*Corresponding author. E-mail: oolafadehan@unilag.edu.ng.

bodies are worrisome and of great concern (Derakhshan et al., 2013) owing to their potent obstinately color and great amount of biochemical oxygen demand that is non-aesthetical to the environment (Annadurai and Krishnan, 1997). Many of these dye wastes pose serious hazards to aquatic living organisms for reason of their toxicity and even carcinogenicity and mutagenic influence on human beings. Equally, there is a reduced penetration of light as a result of their presence in water bodies thereby preventing the aqueous fauna and flora photosynthesis (Elizalde-González and Hernández-Montoya, 2009). A typical example of such dyes is methylene blue (a heterocyclic aromatic chemical compound), which is reported to be responsible for a number of health issues such as eye burn, regurgitation, shock, blue discoloration of the skin (that is, cyanosis), yellowness of the eyes, skin and urine (that is, icterus), high heart rate, among others, with much acute exposure. Consequently, environmental regulations have been enacted by many governments concerning the quality of colored effluents and thus the dye-industries have been compelled to decolorize these colored effluents before they are being discharged into the environment. Hence, much attention should be given to the treatment of dyes before discharge. However, dye producers and users generate dyestuff that is somewhat not easy to degrade after utilization. Attempt to remove them from industrial wastewater by employing the conventional treatment technologies such as trickling filter, liquid-liquid extraction, membrane filtration, chemical coagulation, activated sludge, carbon adsorption and photodegradation, whose extensive review has been provided by Vandevivere et al. (1998), is financially demanding due to their resistant biodegradable complex structure (Afroze et al., 2015; Khodaie et al., 2013). Among these treatment techniques, adsorption is highly employed owing to its flexibility, ease of operation, high performance and relatively inexpensive use, efficient regeneration and eco-friendly operating system (Vakili et al., 2014). It can equally manage quite high flow rates. Hence, during the photodegradation of wastewater-containing dyes using ultra-violet light, the generation of obnoxious substances, such as free radicals and ozone, is mitigated so that high-quality effluent results (Wang et al., 2013). Moreover, adsorption process is still a relevant and comparatively simple, viable and less expensive among other unit operations. However, its effectiveness depends largely on the adsorbents applied and the operating conditions of the process.

Many investigators have reported dyes adsorption on different adsorbents such as peat (Poots et al., 1976), wood (Poots et al., 1976; Asfour et al., 1985a; 1985b; El-Geundi, 1991), pith (McKay, 1987), activated carbon (Walker and Weatherley, 1997; Namasivayam et al., 2001a; Namasivayam and Kavitha, 2002), waste red mud (Namasivayam and Arasi, 1997; Namasivayam et al., 2001b; Namasivayam et al., 2002), fuller's earth (Atun et al., 2003), bottom ash and de-oiled soya (Mittal et al., 2010), copper oxide nanoparticle-modified activated carbon (Nekouei et al., 2015), and synthesized novel adsorbent of ZnO-NR-activated carbon (Dil et al., 2016). Other commercially-potentially adsorbents employed to treat industrial wastewater containing dyes are agricultural byproducts (Namasivayam and Kavitha, 2002; Marshall and Champagne, 1995; Marshall and Johns, 1996), miswak leaves (Elmorsi, 2011), titanium (IV) oxide surface (Gupta et al., 2011), multi-walled carbon nanotubes and titanium (IV) oxide (Saleh and Gupta, 2014). Equally, mercury-doped zinc (II) oxide nanorods (Saravanan et al., 2013a), ZnO/CuO nanocomposites (Saravanan et al., 2013b), CeO_2, V_2O_5, CuO and nanocomposite of CeO_2/V_2O_5 and CeO_2/Cu (Saravanan et al., 2013c) and zinc (II) oxide/silver nanocomposite (Saravanan et al., 2013d) have been applied for the adsorption of dyes. Also, adsorbents for the treatment of dye contaminated aqueous solution include Fe_3O_4 nanoparticles (Ghaedi et al., 2015), zinc (II) oxide/silver/Mn_2O_5 nanocomposite (Saravanan et al., 2015), carbonaceous material (Gupta et al., 2016), ZnO/CeO_2 nanoparticles (Saravanam et al., 2016), commercially used bast fibers under the names of flax, ramie and kenaf (Kyzas et al., 2018) and activated carbon coated with zinc oxide (Pourali et al., 2020). In particular, adsorbents that have been utilized for methylene blue adsorption from aqueous solution include jute fiber carbon (Senthilkumaar et al., 2005), unburned carbon (Wang et al., 2005), cedar sawdust and crushed brick (Hamdaoui, 2006), bamboo activated carbon (Hameed et al., 2007), garlic peel (Hameed and Ahmad, 2009), bentonite (Hong et al., 2009) and carbon nanotube (Yao et al., 2010). Nevertheless, some of these adsorbents showed a low-level property of methylene adsorption and have the drawbacks of inefficacious extraction of MB (Sun et al., 2011). Moreover, almost all of them become problematic with regard to recycling and reuse. Thus, a high-performance, inexpensive and easily-regenerated adsorbent is highly preferred.

In general, non-synthetic and sustainable materials are being used as cost-effective adsorbents in the process of adsorption. Biosorbents have gained wide attention owing to their somewhat plenteousness and non-toxic nature (Tran et al., 2015). Natural polymer biosorbents (such as polysaccharides, that is, chitosan and its precursor, chitin) have been favorably utilized in adsorption studies (Sarode et al., 2019). The second naturally available biopolymer after cellulose is chitin. The application of chitosan typically those derived from crustacean sources are presently considered as a good replacement for charcoal due to their high adsorption capacities under favorable conditions. However, the application of chitin on a commercial scale is limited owing to its poor solubility. Hence, soluble chitosan has been obtained from chitin by an alkaline deacetylation process (Hamed et al., 2016; Muxika et al., 2017). Chitosan is

an efficacious biosorbent for the removal of a number of contaminants owing to its reactive functional groups, amine and hydroxyl groups, enriched-structure (Sharififard et al., 2018). Thus, for reason of their intrinsic characteristics, the non-synthetic polymers are usually deployed as effective biosorbents for the removal or the recovery of hazardous dyes, proteins, heavy metals, amongst others (Fan et al., 2012). So, the evaluation of adsorption capacity of chitosan from diverse sources is an area of great interest to many researchers. Chitosan has been applied in the literature (Annadurai et al., 1999; Hu et al., 2006; Annadurai et al., 2008; Hasan, 2008; Wan Ngaha et al., 2011; Fan et al., 2013; Periolatto and Ferrero, 2013; Li et al., 2014; Sheshmani et al., 2014; Shajahan et al., 2017; Ahmed et al., 2020; da Silva Alves et al., 2021) as an adsorbent for the removal of dyes from aqueous solution. However, to the best of our knowledge, none of these studies carried out an extensive investigation on the modeling of the equilibrium data of the adsorption of methylene blue on chitosan flakes from *Archachatina marginata* shell powder using 19 isotherms and 8 kinetic models coupled with statistical criteria and sum of normalized error (SNE) to select the best models. Hence, the present study reports comprehensively the adsorption of methylene blue (MB) on the prepared chitosan from *A. marginata* shell powder. The effects of operational parameters such as adsorbent dosage, pH of methylene blue solution, initial concentration of MB solution, contact time and temperature on the % removal of MB and adsorption capacity of the chitosan flakes were investigated. The fit of the experimental equilibrium adsorption data of MB to seven 2-p, eight 3-p, three 4-p and one 5-p isotherms were exhaustively carried out in this study, wherein the inherent parameters in the 19 isotherms were evaluated using linear and non-linear methods, as the case may be, to convincingly reflect the surface properties and by extension the adsorption capacity of the chitosan flakes from *A. marginata* shell powder. The kinetics of the adsorption of MB on chitosan flakes was investigated using 8 kinetic models. Moreover, sum of normalized error (*SNE*) was used to opt the most superior models amongst the isotherms and kinetic models for the adsorption of MB on chitosan flakes since *SNE* has been reported as a way or criterion for selecting the best fitted isotherm/kinetic model (Anirudhan and Radhakrishnan, 2009; Yanev et al., 2013; Popoola, 2019). Equally, in this study, Akaike information criteria (*AIC*) and model selection criterion (*MSC*) were used to select the best fitted isotherm and kinetic models for the MB adsorption on the prepared chitosan flakes. Thermodynamic parameters such as activation energy, E_a, changes in enthalpy, ΔH°, entropy, Δs° and Gibbs free energy, ΔG°, were evaluated. The data reported in this study can be of beneficial use for the design and fabrication of an economically viable treatment process using batch reactor for MB adsorption on a biosorbent and for diluting industrial effluents.

MATERIALS AND METHODS

The analytical grade chemical reagents used in this study included NaOH pellet (99.8% purity), obtained from Merck, India and methylene blue ($C_{16}H_{18}N_3SCl$), whose molecular weight and purity are 319.85 g/mol and 98.7%, respectively, procured from Loba Chemie PVT Limited, India, ethanol (absolute 98%), hydrochloric acid (36.5-38%, specific gravity=1.18) and acetone, $CH_3C{=}O$ ($\geq$ 99.5% ACS), which were procured from BDH Laboratories Supplies, England. These chemicals were used without additional treatment.

Production of biosorbent

The production of the biosorbent (chitosan) used in this study from the shell wastes of *A. marginata* (African giant snail) was performed by washing the shell, drying, pulverization and following the processes of demineralization, deproteinization, deacetylation and decolorization as detailed in the works of Amoo et al. (2019), Olafadehan et al. (2020; 2021) and Bello and Olafadehan (2021).

Characterization of biosorbent

The characterization of the resulting flakes of chitosan was extensively carried out and reported elsewhere (Bello and Olafadehan, 2021). In this study, the surface point of zero charge of the prepared chitosan flakes from *A. marginata* shell was performed using the pH drift method as adopted by Banerjee and Chattopadhyaya (2013) with slight modification. 0.1 M NaCl solution was freshly prepared and 50 mL was placed in a series of 250 mL Erlenmeyer flasks and various values of pH between 2 and 12 were initiated using 0.1 M HCl and 0.1 M NaOH solutions monitored by a sensitive pH meter. 0.1 g of the chitosan flakes was discharged into the solution, which was allowed to reach equilibrium in 24 h. The solutions were filtered and the difference between the initial pH values $(pH)_i$ and final pH values, $(pH)_f$ was evaluated to obtain change in pH values, $\Delta(pH)$. The $\Delta(pH)$ values were plotted against $(pH)_i$ values. The point of intersection of the curve with the abscissa, $(pH)_i$, gives the zero-point charge value, pH_{zpc}.

Preparation of methylene blue solution

A stock solution of 1000 mg/L of methylene blue (MB) was prepared by dissolving a weighed portion of 1 g of it in 1000 cm^3 (or 1 L), from which various concentrations were obtained by serial dilution.

Batch adsorption experiment

The batch adsorption experiment considered the operational effects of adsorbent dosage, pH of MB solution, initial concentration of MB solution, contact time and temperature on the methylene blue adsorption on the prepared chitosan flakes. Each 50 mL sample of methylene blue solution was put in 250 mL capacity of Erlenmeyer flasks at specific or certain conditions. The effect of adsorbent dosage on the % removal of MB and adsorption capacity of the chitosan was studied by using the mass of the biosorbent between 0.1 and 2 g. The influence of pH was investigated in acidic and

alkaline medium by varying pH values using 0.1 M HCl and 0.1 M NaOH measured by a pH meter. The effect of initial concentration of MB solution on the % removal of methylene blue (MB) was investigated by using 10 to 60 mL with a fixed amount of 0.1 g of biosorbent (chitosan) at contact time of 30 min, agitated using a mechanical orbit shaker set at 120 rev/min and ambient temperature of 30 ± 2°C. The impact of contact time was carried out within 4 h durations at a fixed mass of 0.1 g chitosan and room temperature of 30 ± 2°C. The thermodynamics study, which is hinged on the effect of variation of temperature, was carried out in water bath within the temperature ranges of 30 to 90°C at a fixed adsorbent amount of 0.1 g.

At the end of each adsorption operational batch experiments, chitosan flake particles were filtered from the suspension and the final concentration was measured by ultra-visible spectrophotometer at maximum wavelength of 650 nm.

Adsorption equilibrium isotherms

An adsorption isotherm is an empirical equation that solely gives an insight of the mechanism or phenomenon that revolves round the retention or release of a liquid phase (adsorbate) on a solid phase (adsorbent) at constant temperature (Deng and Chen, 2019). The adsorption process is said to have attained equilibrium when the adsorbate and adsorbent have been sufficiently contacted and adsorbate concentration in the bulk solution is in a dynamic balance with the interface concentration (Magdy et al., 2018). This present study uses two-, three-, four- and five- parameter isotherms to model the equilibrium sorption data of methylene blue on chitosan flakes using linear and non-linear regression methods, where appropriate.

2-p Freundlich isotherm

The 2-p Freundlich isotherm assumes a reversible adsorption that is not limited to the formation of monolayer, non-uniform distribution of heat of adsorption, heterogeneous adsorbate surface without lateral interaction and initial stronger binding sites, which reduce with increase of coverage. The empirical equation of Freundlich isotherm is of the form (Freundlich, 1906):

$$q_e = k_F c_e^{1/N} \quad (1)$$

where q_e is the weight of adsorbate adsorbed per unit weight of adsorbent at equilibrium (mg/g), c_e the residual concentration of the solute (mg/L) and k_F is a constant depending on the adsorbate and the adsorbent: it indicates the Freundlich adsorption capacity (Benzaoui et al., 2018) and the parameter, N, characterizes the homogeneity of the system (that is, the favorability of adsorption). A larger *N* value is an indication that that the system is more heterogeneous that usually results in the non-linearity of the adsorption isotherm.

Taking natural logarithms of Equation 1, we have:

$$In\ q_e = In\ k_F + \frac{1}{N} In\ c_e \quad (2)$$

The linear plot of $In\ q_e$ against $In\ c_e$ is used to test the fitness of equilibrium data to the Freundlich isotherm provided $N > 1$ and a high correlation coefficient, R^2, close to unity is obtained. Thus, the Freundlich isotherm parameters, N and k_F, can be determined from the slope $(= 1/N)$ and intercept on $In\ q_e$ axis $(= In\ k_F)$, respectively. The values of *N* between 1 and 10 are used to assess the adsorbent-adsorbate interaction (Kumar et al., 2012). The magnitude of the exponent, 1/*N*, is a measure of the nature of the adsorption process. When $1/N = 0$, the adsorption is irreversible. The adsorption is favorable (that is, indicative of chemisorption) when $0 < 1/N < 1$. It is also indicative of chemisorption and unfavourability when $1/N > 1$. Hence, if $1 < N$, favorable (or cooperative) adsorption results (Pandey and Mishra, 2011). The empirical constant, *N*, which indicates adsorption intensity, depends on the temperature and properties of the adsorbate and the adsorbent.

2-p Langmuir isotherm

Langmuir (1918) proposed an empirical model, which assumes complete monolayer adsorption, limited number of active sites, voidance of lateral interaction, homogeneous adsorbent surface with identical adsorption sites and constant heat of adsorption for all sites. The 2-p Langmuir isotherm, when applied to liquid phase adsorption, is given by:

$$q_e = \frac{q_{max} K_L c_e}{1 + K_L c_e} \quad (3)$$

where q_{max} is the Langmuir constant related to the adsorption capacity (that is, maximum adsorption capacity for the solid phase loading) (mg/g) and K_L the energy constant related to the heat of adsorption (L/mg). q_{max} can be correlated with the variation of the suitable area and porosity of the adsorbent. Hence, large surface area and pore volume result in higher adsorption capacity of the adsorbent (Olafadehan, 2021).

Five different linear forms can result from Equation 3. One of such forms used in this study is given by:

$$\frac{c_e}{q_e} = \frac{1}{q_{max}} c_e + \frac{1}{q_{max} K_L} \quad (4)$$

The linear plot of (c_e/q_e) against c_e should yield a straight line with a high coefficient of regression, R^2, being close to unity if the adsorption process was described by the model. The inherent parameters, q_{max} and K_L, in the 2-p Langmuir isotherm can thus be determined from the slope $(= 1/q_{max})$ and intercept on (c_e/q_e) axis $(= 1/(q_{max} K_L))$ respectively.

Hall et al. (1966), Weber and Chakkravortic (1974) and Malik (2004) described the essential attributes of the Langmuir model using a dimensionless constant referred to as separation factor or equilibrium parameter, R_L, given by Mahmoud et al. (2016) thus:

$$R_L = \frac{1}{1+K_L c_0} \quad (5)$$

The factor, R_L, describes the nature of adsorption within a certain limit as either irreversible for $R_L < 1$, favorable for $0 < R_L < 1$, linear for $R_L = 1$ and unfavorable for $R_L > 1$ (Zhai et al., 2004).

2-p Temkin isotherm

The Temkin isotherm assumes that the heat of adsorption, ΔH_{ads}, of the molecules at the surface of the adsorbent decreases linearly rather than logarithmically with coverage θ, that is, $\Delta H_{ads} = (\Delta H_{ads})_0 (1-\theta)$; homogeneous distribution of binding energies of the adsorbent surface and it takes cognizance of the adsorbate-adsorbent surface interaction (Temkin and Pyzhev, 1940). The 2-p Temkin isotherm is given by:

$$q_e = \frac{RT}{b_T} In(A_T c_e) = \frac{RT}{b_T}(In A_T + In c_e) \quad (6)$$

where b_T is Temkin constant, which is related to the heat of adsorption (J/mol) and A_T the Temkin isotherm constant (L/g). A plot of q_e against $In c_e$ should be a straight line with slope equals RT/b_T and intercept on q_e axis = $RT\ In A_T / b_T$. Hence, the two parameters, b_T and A_T, of the isotherm can be determined at the temperature of adsorption.

2-p Dubinin-Radushkevich (D-R) isotherm

The mechanism for adsorption can be expressed with a Gaussian energy distribution onto a heterogeneous surface using the 2-p Dubinin-Radushkevich model (Celebi et al., 2007; Gunay et al., 2007). It assumes a multilayer physical adsorption process that involves van der Waal's forces and is a fundamental equation that is used qualitatively for the description of the adsorption of gases and vapors onto microporous sorbents (Israel and Eduok, 2012). The 2-p Dubinin-Radushkevish isotherm is expressed as:

$$q_e = q_{DR} \exp(-\beta \varepsilon^2) \quad (7)$$

In linear form, Equation 7 becomes:

$$In\, q_e = In\, q_{DR} - \beta \varepsilon^2 \quad (8)$$

The approach was often applied to distinguish between the physisorption and chemisorption of metal ions (Dubinin, 1960; Vijayaraghavan et al., 2006), with its mean free energy, *E*, per molecule of adsorbate (for removing a molecule from its location in the adsorption space to infinity) given by:

$$E = 1/\sqrt{2\beta} \quad (9)$$

The Polanyi potential, ε, is given by:

$$\varepsilon = RT\ In(1 + c_e^{-1}) \quad (10)$$

Using Equation 10 in Equation 8, a linear plot can be made to determine the relevant constants inherent in Dubinin-Radushkevich isotherm.

2-p Harkins-Jura (H-J) isotherm

The 2-p Harkins-Jura model accounts for the adsorption of multilayer on the surface of adsorbents having heterogeneous pore distribution. The non-linear relationship of Harkins-Jura isotherm is given by:

$$q_e = \sqrt{\frac{A_{HJ}}{B_{HJ} - \log c_e}} \quad (11)$$

where A_{HJ} and B_{HJ} are the isotherm constant parameters. On linearization of Equation 11, we have:

$$\frac{1}{q_e^2} = \frac{B_{HJ}}{A_{HJ}} - \frac{1}{A_{HJ}} \log c_e \quad (12)$$

Therefore, a straight line should be obtained from the plot of $1/q_e^2$ against $\log c_e$, which is adequate to determine the isotherm parameters, A_{HJ} and B_{HJ}, from slope = $1/A_{HJ}$ and intercept on vertical axis = B_{HJ}/A_{HJ}.

2-p Frenkel-Halsey-Hill (F-H-H) isotherm

The 2-p Frenkel-Halsey-Hill assumes a multilayer adsorption on a heterogonous adsorbent surface. Its non-linear form is expressed as:

$$q_e = exp\left(\frac{In K_{FHH} - In c_e}{n_{FHH}}\right) \quad (13)$$

whose linear form is given by:

$$In\, q_e = \frac{1}{n_{FHH}} In K_{FHH} - \frac{1}{n_{FHH}} In c_e \quad (14)$$

Therefore, a straight line should be obtained from the plot of $In\, q_e$ against $In\ c_e$, which suffices to determine the isotherm parameters, n_{FH} and K_{FH}, from slope = $1/n_{FHH}$ and intercept on the vertical axis = $In K_{FHH}/n_{FHH}$.

Brunauer-Emmett-Teller (BET) isotherm

The Brunauer-Emmett-Teller (BET) model is a notable representation of multilayer adsorption. It assumes that the adsorbate-adsorbent surface interaction is much larger than

between neighboring molecules, the possession of homogeneous chemical properties by the adsorbent and it is applied generally for estimating the surface area of porous media (Chen et al., 2017). The non-linear form of BET isotherm is expressed as (Olafadehan, 2021):

$$q_e = \frac{q_s c_{BET} c_e}{\left(c_s - c_e\right)\left[1+\left(c_{BET}-1\right)\left(\frac{c_e}{c_s}\right)\right]} \quad (15)$$

where c_s is the adsorbate monolayer saturation concentration, q_s the amount of solute adsorbed in forming a complete monolayer (mg/g) and c_{BET} indicates a constant that explains the energy of interaction with the surface.

The linearized form of Equation 15 is given thus:

$$\frac{c_e}{q_e\left(c_s - c_e\right)} = \frac{1}{q_s c_{BET}} + \frac{\left(c_{BET}-1\right)}{q_s c_{BET}}\left(\frac{c_e}{c_s}\right) \quad (16)$$

Equation 16 serves as a two-parameter BET isotherm (designated as BET1 in this current study) if the monolayer saturation concentration, c_s, was considered as a constant value (Agarwal et al., 2014; Rahmi et al., 2018; Gupta and Kumar, 2019; Sabar et al., 2020) and a three-parameter BET isotherm as a curve fitting value (designated as BET2 in this study). According to Ebadi et al. (2009), to eliminate the discrepancies associated with the value of monolayer saturation concentration widely reported, a new or modified 3-parameter BET equation was developed (designated as BET3 in this study), represented as:

$$q_e = \frac{q_m K_s c_e}{\left(1-K_L c_e\right)\left(1-K_L c_e + K_s c_e\right)} \quad (17)$$

where K_L is the equilibrium constant of adsorption of upper layers in BET3 isotherm (L/mg) and K_s the equilibrium constant of adsorption for the first layer in Langmuir and BET isotherms (L/mg).

3-p Redlich-Peterson isotherm

The 3-p Redlich-Peterson isotherm, given in Equation 18, fuses the Langmuir and Freundlich isotherms into a single equation (Redlich and Peterson, 1959).

$$q_e = \frac{k_{RP} c_e}{1+\alpha_{RP} c_e^{\beta_{RP}}} \quad (18)$$

where k_{RP} and α_{RP} are the Redlich-Peterson isotherm constant parameters of units L/g and L/mg, respectively and $0 < \beta_{RP} < 1$. For $\beta_{RP} = 0$ and $\beta_{RP} = 1$, Equation 18 reduces to Henry's law (or linear adsorption) and Langmuir isotherm, respectively.

Rearranging and linearizing Equation 18, we have:]

$$\frac{c_e}{q_e} = \frac{1}{k_{RP}} + \left(\frac{\alpha_{RP}}{k_{RP}}\right) c_e^{\beta_{RP}} \quad (19)$$

The inherent parameters in the Redlich-Peterson isotherm are determined by minimizing the sum of squares of errors between the $\left(q_e\right)_{expt}$ and $\left(q_e\right)_{pred}$ values using $0 < \beta_{RP} < 1$ when a plot of $\left(c_e/q_e\right)$ versus c_e is made with slope $\left[=\left(\alpha_{RP}/k_{RP}\right)\right]$ and intercept on vertical axis $\left[=\left(1/k_{RP}\right)\right]$.

3-p Tóth isotherm

The 3-p Tóth model arises from the potential theory and is mainly appropriate to describe heterogeneous adsorption systems that satisfy both low- and high-end boundaries of adsorbate concentration (Padder and Majumder, 2016). It is hinged on the presupposition of possession of a quasi-Gaussian energy distribution of the adsorbent sites, that is, the sites predominantly have adsorption energies lower than the maximum adsorption (Tóth, 1971; Padmesh et al., 2006). The non-linear form of Tóth isotherm is represented thus:

$$q_e = \frac{q_m K_T c_e}{\left[1+\left(K_T c_e\right)^{\beta_T}\right]^{1/\beta_T}} \quad (20)$$

where K_T and β_T are the Tóth isotherm constants, which are both expressed in (mg/g). The heterogeneity of the adsorption system is characterized by the parameter, β_T (Behbahani and Behbahani, 2014). The adsorption system is said to be heterogeneous if β_T is not close to 1. The parameters, q_m, K_T and β_T, of the Tóth isotherm can be estimated by non-linear regression analysis.

3-Sips isotherm

The 3-p Sips isotherm model assumes localized adsorption void of interactions between adsorbates and fuses the Langmuir and Freundlich expressions patterned to predict the behavior of heterogeneous adsorption systems. This model eradicates the Freundlich model limitation at high concentration of adsorbate but rather gives the prediction of a monomolecular layer adsorption capacity of Langmuir isotherm and is uniquely transformed to the isotherm of Freundlich at low adsorbate concentration. The non-linear Sips isotherm is expressed thus:

$$q_e = \frac{q_{SP} K_{SP} c_e^{\beta_s}}{1+K_{SP} c_e^{\beta_s}} \quad (21)$$

where q_{SP} and K_{SP} are the Sips isotherm model constant and $\beta_S\left(=1/N\right)$is the Sips isotherm exponent. These isotherm parameters are determined using non-linear regression analysis.

3-p Khan isotherm

The 3-p Khan model, which was developed originally for bi-

adsorbate from simulated or pure dilute solutions, combines the features of Langmuir and Freundlich isotherms. The non-linear Khan isotherm is given by (Amrhar et al., 2015a, b):

$$q_e = \frac{q_{max} b_K c_e}{a_K \left(1 + b_K c_e\right)} \tag{22}$$

where q_{max} is the Khan isotherm maximum adsorption capacity (mg/g), a_K the Kahn isotherm exponent and b_K the Khan isotherm constant.

Linearizing Equation 22, we have:

$$\frac{1}{q_e} = \left(\frac{a_K}{q_{max} b_K}\right)\frac{1}{c_e} + \frac{a_K}{q_{max}} \tag{23}$$

Therefore, a straight line should be obtained from the plot of $1/q_e$ against $1/c_e$, with slope $= a_K / \left(q_{max} b_K\right)$ and intercept on vertical axis $= a_K / q_{max}$. Thus, the general expression for the Kahn isotherm can be obtained using Equation 22. However, non-linear regression method is employed to determine the three Khan isotherm model parameters, q_{max}, a_K and b_K.

3-p Radke-Prausnitz isotherm

The 3-p Radke-Prausnitz model is basically applied for broad range of concentration and is widely used for adsorption systems at low concentration (Ramadoss and Subramaniam, 2018). It is expressed as:

$$q_e = \frac{q_{max} K_{RPI} c_e}{\left(1 + K_{RPI} c_e\right)^{\alpha_{RPI}}} \tag{24}$$

where q_{max} is the Radke-Prausnitz maximum adsorption capacity (mg/g), K_{RPI} the Radke-Prausnitz equilibrium constant and α_{RPI} the Radke-Prausnitz model exponent. The Radke-Prausnitz model parameters, q_{max}, K_{RPI} and α_{RPI} can be obtained by non-linear statistical fit of experimental data.

3-p Fritz-Schlüender isotherm

The 3-p Fritz-Schlüender isotherm is a model that incorporates the features of Langmuir and Freundlich isotherms and it utilizes three parameters that fit a wide range of experimental data. It is expressed as (Ramadoss and Subramaniam, 2018):

$$q_e = \frac{\left(q_m\right)_{FS} K_{FS} c_e}{1 + \left(K_{FS} c_e\right)^{\alpha_{FS}}} \tag{25}$$

where $\left(q_m\right)_{FS}$ is Fritz-Schlüender maximum adsorption capacity, K_{FS} the Fritz-Schlüender equilibrium constant and α_{FS} the Fritz-Schlüender isotherm exponent. The 3-p Fritz-Schlüender isotherm parameters can be determined by non-linear regression analysis.

4-p Fritz-Schlüender isotherm

The 4-p Fritz-Schlüender is an empirical model that integrates the Langmuir and Freundlich isotherms and is given thus (Hamdaoui and Naffrechoux, 2007):

$$q_e = \frac{A_{FS} c_e^{\Phi_{FS}}}{1 + B_{FS} c_e^{\beta_{FS}}} \tag{26}$$

The model is valid only when Φ_{FS} and $\beta_{FS} \leq 1$. The 4-p Fritz-Schlüender isotherm parameters can be determined by non-linear regression analysis.

4-p Bauder isotherm

The 4-p Bauder model was borne out of the need to accurately account for the differences in the course of calculating Langmuir constant and coefficient over a wide range of certain specifications linked to its parameters. It is given by:

$$q_e = \frac{\left(q_m\right)_B b_0 c_e^{1+x+y}}{1 + b_0 c_e^{1+x}} \tag{27}$$

where $\left(q_m\right)_B$ is Bauder maximum adsorption capacity, b_0 the Bauder equilibrium constant, *x* and *y* are the Bauder isotherm parameters. Owing to the inherent bias resulting from linearization, the 4-p Bauder isotherm parameters can be obtained by non-linear regression analysis. However, its application must satisfy the conditions of $\left(1 + x + y\right) < 1$ and $\left(1 + x\right) < 1$.

4-p Marczewski-Jaroniec isotherm

The 4-p Marczewski-Jaroniec model considers the local Langmuir isotherm and takes into cognizance the distribution of adsorption energies associated with the active sites of adsorbent for low and high value cases of the process. It is expressed as (Ayawei et al., 2017):

$$q_e = \left(q_m\right)_{MJ}\left[\frac{\left(K_{MJ} c_e\right)^{\alpha_{MJ}}}{1 + \left(K_{MJ} c_e\right)^{\alpha_{MJ}}}\right]^{\beta_{MJ}/\alpha_{MJ}} \tag{28}$$

where $\left(q_m\right)_{MJ}$ is Marczewski-Jaroniec maximum adsorption capacity, K_{MJ} the Marczewski-Jaroniec equilibrium constant, the heterogeneity of the adsorbent surface is characterized by the Marczewski-Jaroniec isotherm parameters, α_{MJ} and β_{MJ}: α_{MJ} and β_{MJ} give the description of the spreading of distribution in the path of less and higher adsorption energies respectively. The 4-p Marczewski-Jaroniec isotherm parameters, $\left(q_m\right)_{MJ}$, K_{MJ}, α_{MJ}

and β_{MJ}, are obtained by non-linear regression analysis.

5-p Fritz-Schlüender isotherm

The 5-p Fritz-Schlüender isotherm was proposed to simulate accurately variations in isothermic model such that it can be applied over a large range of equilibrium data. It is given by:

$$q_e = \frac{(q_m)_{FS5} K_{FS5} c_e^{\alpha_{FS5}}}{1+\Phi_{FS5} c_e^{\beta_{FS5}}} \quad (29)$$

where $(q_m)_{FS5}$ is Fritz-Schlüender maximum adsorption capacity. The 5-p Fritz-Schlüender isotherm parameters, $(q_m)_{FS5}$, K_{FS5}, Φ_{FS5}, α_{FS5} and β_{FS5}, are estimated by non-linear regression analysis.

Batch reactor design

The aim of the prototype is to determine the mass of the prepared chitosan flakes (adsorbent), *m*, required to remove the adsorbate (methylene blue) from solution of volume, *V*, at near real environmental initial concentration of c_0 to relatively allowable levels of concentration, c_e. However, the design of single solute batch adsorption systems can be facilitated by adsorption isotherms and equilibrium data. Based on the applicable adsorption isotherm, the mass of adsorbent required to realize specified percentage removal efficiency, *R*, from aqueous solution of volume *V* for a known initial concentration of the adsorbate, except for 100% removal efficiency, is derived in this study. The adsorption percentage, R, adsorption capacity values at equilibrium, q_e, and at time *t*, q_t, are determined using Equations 30 to 32, respectively:

$$R = \left(\frac{c_0 - c_e}{c_0}\right) \times 100 \quad (30)$$

where c_0 is initial concentration of methylene blue solution (adsorbate), and c_e the concentration of adsorbate at equilibrium, both of units, mg/L.

$$q_e = \left(\frac{c_0 - c_e}{m}\right) V \quad (31)$$

$$q_t = \left(\frac{c_0 - c_t}{m}\right) V \quad (32)$$

where c_t is the concentration of adsorbate at time *t*, expressed in mg/L, *m* the mass of adsorbent (g), V volume of aqueous solution in contact with the adsorbent (L).

From Equation 30, we obtain:

$$c_e = c_0(1 - R/100) \quad (33)$$

Combining Equations 30 and 31, we have:

$$q_e = RVc_0/100m \quad (34)$$

Equations 33 and 34 can now be used in the isotherm that correlates the equilibrium adsorption data to determine the mass of adsorbent required to achieve certain percentage removal of adsorbate from solutions of varied volumes (say, 1-20 L) at ambient temperature in a mono-solute batch reactor system. Olafadehan (2021) obtained Equation 35 assuming the adsorption equilibrium data are correlated using Langmuir isotherm.

$$m = \frac{V \times R \times c_0 \{1 + K_L \{c_0 [1 - (R/100)]\}\}}{100 q_{max} K_L \{c_0 [1 - (R/100)]\}} \quad (35)$$

Adsorption kinetics

The adsorption kinetics describes rate of uptake of the solute, which, in turn, influences the residence time of the uptake of the adsorbate at the solid-solution interface. Thus, it is imperative to understand the reaction mechanism for the sorption process in a bid to design appropriately the sorption treatment plants. So, the adsorption kinetics is a major issue in the design of a treatment system using adsorbent. Moreover, it is used to establish the controlling step in an adsorption process. Adsorption kinetics provides information to relational industry operators and planners that can be used to effectively treat the contaminated wastewater by adsorption since rapid adsorption of the solute in an adsorption system is desirable and beneficial for actual or industrial applications. The kinetic parameter, which aids the prediction of the rate of adsorption and equilibrium time, gives significant information for designing and modeling the adsorption processes (Sivarajasekar and Baskar, 2014). The adsorption kinetics investigated in this study are illustrated in the following.

Fractional power model

The fractional power model can be expressed in the form of Freundlich equation, which indicates that the uptake of the adsorbate (or solute) increases exponentially with time. It is given by:

$$q_t = k_f t^{\nu} \quad (36)$$

where q_t is the amount of solute adsorbed per weight of adsorbent at time *t* (mg/g); ν the fractional order, k_f is the fractional power kinetic model constant (mg/(g min$^{\nu}$)) and *t* time of adsorption (min).

Taking natural logarithms of Equation 36 gives:

$$In\, q_t = In\, k_f + \nu In t \quad (37)$$

Therefore, a plot of $In\ q_t$ against $In\ t$ can be made to determine the parameters, ν and k_f, from the slope and intercept on the vertical axis, respectively.

Lagergren pseudo first-order kinetic model

The Lagergren pseudo first-order kinetic model, expressed in Equation 38, describes the adsorption of solutes onto adsorbents following the first-order mechanism (Ho, 2004):

$$\frac{dq_t}{dt} = k_1(q_e - q_t) \tag{38}$$

where k_1 the Lagergren pseudo first-order rate constant (min^{-1}).

The integral of Equation 38 from $t=0$, $q_t=0$ to $t=t$, $q_t=q_t$ yields the non-linear form:

$$q_t = q_e\left(1-e^{-k_1 t}\right) \tag{39}$$

The linearized form of Equation 39 is:

$$In\left(q_e - q_t\right) = In\, q_e - k_1 t \tag{40}$$

Therefore, a straight line should be obtained from the plot of $In\left(q_e - q_t\right)$ against t, which is adequate to determine k_1.

Pseudo second-order kinetic model

The pseudo second-order kinetic model assumes the adsorption of solutes onto adsorbents follows the second-order mechanism and is given by:

$$\frac{dq_t}{dt} = k_2(q_e - q_t)^2 \tag{41}$$

where k_2 is the specific reaction rate constant for the pseudo second-order kinetics (g/(mg min)), which can be used to calculate the initial sorption rate, h, [=] mg/(g min) thus:

$$h = k_2 q_e^2 \tag{42}$$

When integrated, Equation 41 yields:

$$q_t = \frac{k_2 q_e^2 t}{1 + k_2 q_e t} \tag{43}$$

Linearization of Equation 43 yields different forms. One of such linear forms employed in this study is:

$$\frac{t}{q_t} = \frac{1}{k_2 q_e^2} + \frac{t}{q_e} \tag{44}$$

Therefore, a straight line should be obtained from the plot of $\left(t/q_t\right)$ against *t*, which is adequate to determine k_2.

Elovich kinetic model

The Elovich kinetic model describes adsorption process in a non-ideal state and on chemisorption phenomena (Gupta and Kumar, 2019) and is given by:

$$\frac{dq_t}{dt} = \alpha \exp\left(-\beta q_t\right) \tag{45}$$

where α and β are constants during an experiment. As $q_t \to 0,\ dq_t/dt \to \alpha$. Hence, α is regarded as the initial rate of adsorption. Equation 45, when integrated using the conditions $t=0,\ q_t=0$ and $t=t,\ q_t=q_t$, yields:

$$q_t = \frac{1}{\beta}\left[In\left(t+\Phi\right) - In\,\Phi\right] \tag{46}$$

where $\Phi = 1/(\alpha\beta)$. If $t >> \Phi$, Equation 46 simplifies to:

$$q_t = \frac{1}{\beta} In(\alpha\beta) + \frac{1}{\beta} In\, t \tag{47}$$

Therefore, a straight line should be obtained from the plot of q_t against $In\,t$ to check if $t >> \Phi$ for the coefficient of determination, R^2, should be greater than 1. This allows the determination of β (g/mg) and α (mg/(g min)) from the slope and intercept on vertical axis respectively.

Avrami kinetic model

The Avrami kinetic model, also known as the Johnson-Mehl-Avrami-Kolmogorov (JMAK) model, was first derived by Kolmogorov et al. (1937) and popularized by Avrami (1939, 1940, 1941). The Avrami kinetic model assumes random nucleation sites across the reaction surface of the adsorbent and it evaluates changes in kinetic parameters as function of reaction time and temperature. The non-linear form of the expression is given as (Ahmad et al., 2014; Yoro et al., 2017):

$$q_t = q_e\left[1 - \exp\left(-k_{AV} t^{n_{AV}}\right)\right] \tag{48}$$

where k_{AV} is the Avrami rate constant ($\min^{-n_{AV}}$) and n_{AV} is a dimensionless constant related to the mechanism of adsorption with regard to temperature and contact time.

Taking the natural logarithms of Equation 48, we have:

$$-In\left(1 - \frac{q_t}{q_e}\right) = k_{AV} t^{n_{AV}} \tag{49}$$

To enable determination of the inherent kinetic parameters in the Avrami kinetic model, another natural logarithmic approach is applied to Equation 49 to yield:

$$In\left[-In\left(1 - \frac{q_t}{q_e}\right)\right] = In\, k_{AV} + n_{AV}\, In\, t \tag{50}$$

which allows the determination of the constants, n_{AV} and k_{AV}, from a plot of $In\left[-In\left(1-\frac{q_t}{q_e}\right)\right]$ against Int. If the transformation followed the Avrami equation, this yields a straight line with slope = n_{AV} and intercept on vertical axis $= In\,k_{AV}$, from which k_{AV} can be determined.

Adsorption is largely over when $\left(q_t/q_e\right)$ reaches values close to 1, which will be at an adsorption time, t_a, defined by $k_{AV}\left(t_a\right)^{n_{AV}} \approx 1$ as then the exponential term in the above expression for $\left(q_t/q_e\right)$ will be small. Thus, adsorption takes a time of order:

$$t_a = 1.0116 \Big/ \left(k_{AV}\right)^{1/n_{AV}} \tag{51}$$

Therefore, adsorption takes a time that decreases as one over the one-quarter power of k_{AV}.

Intraparticle diffusion (IPD) (or Weber-Morris) model

The intraparticle diffusion (IPD) (or Weber and Morris) model, given in Equation 51, is employed to establish the diffusion mechanism involved in the adsorption process.

$$q_t = k_{IPD}\sqrt{t} + C \tag{52}$$

where k_{IPD} is the intraparticle diffusion rate constant (mg/(g min^{½})) and *C* is a constant (mg/g). The intraparticle diffusion rate constant, k_{IPD}, can be estimated from the slope of q_t - $\sqrt{t}$ plot, which ought to be a straight line passing through the origin $(C=0)$ if IPD model could be employed to describe the kinetics of the adsorption process.

The intraparticle diffusion model has attracted many researchers because of the multi-linearity the plot of Equation 52 gives. Malash and El-Khaiary (2010) suggested the use of piecewise regression in expressing adequately the model. The piecewise regression is a special type of linear regression that is used when a single line is insufficient to model a data set marked with multi-linearity. It allows multiple linear models to be fitted to the data for different independent variables. For a two-segment form, the expression is given as:

$$y_i = \beta_0 + \beta_1 x_{i1} + \beta_2\left(x_{i1} - x^{(k)}\right)x_k \tag{53}$$

where x_{i1} is the independent variable value, $x^{(k)}$ the knot value and x_k the knot dummy variable is expressed as:

$$x_k = \begin{cases} 0 & if \;\; x_{i1} \le x^{(k)} \\ 1 & if \;\; x_{i1} > x^{(k)} \end{cases} \tag{54}$$

In this investigation, Equation 52 is tagged IPD-1 segment and Equation 53 is named IPD-2 segment.

Boyd model

Though the Boyd et al. (1947) diffusion model was developed theoretically for ion-exchange kinetics, it had been applied successfully to adsorption studies (Morrison and Boyd, 2004; Castillejos et al., 2011; El-Khaiary and Malash, 2011; Olafadehan et al., 2018) to establish the exact rate-limiting step involved in the adsorption process due to the two-mass transfer processes of solute, which are film and pore diffusion. The Boyd model assumes that the boundary layer surrounding the adsorbent has a greater effect on the diffusion of solute. The Boyd's model is given by:

$$F_B(t) = \frac{q_t}{q_e} = 1 - \frac{6}{\pi^2}\sum_{n=1}^{\infty}\frac{1}{n^2}\exp\left(-n^2 Bt\right) \tag{55}$$

where $F_B(t)$ is dimensionless fraction of solute adsorbed at time *t*, $B = \pi^2 D \Big/ R_p^2$: D the effective intraparticle diffusion coefficient (m^2/s) and R_p radius of adsorbent particle (m).

If intraparticle diffusion was the rate-controlling step in the adsorption process, Equation 52 is valid with $C=0$. Reichenberg (1953) obtained approximate expressions given by Equations 56 and 58 via the application of Fourier transform and then integration of Equation 55:

$$F_B(t) = 1 - \frac{6}{\pi^2}\exp\left(-Bt\right),\; F_B(t) > 0.85 \tag{56}$$

That is,

$$Bt = -In\left[1 - F_B(t)\right] - 0.4977,\; F_B(t) > 0.85 \tag{57}$$

$$Bt = \left(\sqrt{\pi} - \sqrt{\pi - \frac{\pi^2 F_B(t)}{3}}\right)^2,\; F_B(t) \le 0.85 \tag{58}$$

The value of B can be determined using Equation 57 or 58 for each and every value of $F_B(t)$, depending on the conditions given and the Boyd plots (*B*–*t*) constructed (Olafadehan et al., 2018; Ho et al., 2002). The distinction between intraparticle transport-controlled rates of adsorption and the film diffusion (external transport) is revealed by the linearity of the *B*–*t* plots (Olafadehan et al., 2018; Wang et al., 2006). If the adsorption process was controlled by intraparticle diffusion, a straight line passing through the origin would be obtained; otherwise, film diffusion governs the adsorption process (El-Khaiary and Malash, 2011; Olafadehan et al., 2018; Mohan and Singh, 2002; Sharma and Das, 2012).

Diffusion-chemisorption model

The diffusion-chemisorption model assumes that the adsorption or uptake of adsorbate is under the influences of both diffusion and chemisorption. This model was originally used for the uptake of heavy metals on heterogeneous surface (Sutherland and

Venkobachar, 2010). The non-linear form of the diffusion-chemisorption model is given by:

$$\frac{q_e^2}{(q_e - q_t)} = k_{DC}\sqrt{t} + q_e \quad (59)$$

where k_{DC} (mg/(g min$^{-0.5}$)) is the diffusion-chemisorption parameter related to the initial sorption rate, k_i (mg/(g min)) by assuming a linear region as $t \to 0$ using the empirical relationship:

$$k_i = \frac{k_{DC}^2}{q_e} \quad (60)$$

The linear form of Equation 59 amenable for the determination of k_{DC} and q_e by plotting $\sqrt{t}/q_t$ against $\sqrt{t}$ is expressed in Equation 61:

$$\frac{\sqrt{t}}{q_t} = \frac{1}{q_e}\sqrt{t} + \frac{1}{k_{DC}} \quad (61)$$

Error functions

The minimization of the error distribution between the experimental equilibrium data and the predicted isotherms/adsorption kinetics can be determined via error functions' values. Depending on definition of the error function, the error distribution between the experimental equilibrium data and the predicted values is minimized either by the minimization or maximization of the error function. Thus far, no detailed studies are available to compare the accuracy of the error functions in predicting the isotherm/kinetic parameters and also the optimum isotherm/kinetics. The various error functions used in this study for the comparison of the experimental and predicted equilibrium adsorption data are shown in Table 1 where $Q_{k,expt}$ [=$(q_e)_{k,expt}$ or $(q_t)_{k,expt}$] is the measured adsorption data for run *k*, $Q_{k,pred}$ [=$(q_e)_{k,pred}$ or $(q_t)_{k,pred}$] the predicted (or calculated) adsorption data for run *k*, N_e the number of experimental data points and N_p the number of model parameters.

Information-based criteria

The information-based criteria (IC) are criteria for selecting the best fitted isotherm and kinetic model through the use of statistical tools such as Akaike Information Criterion (AIC), Schwarz Bayesian Information Criterion (SBIC), Khinchin's law of Iterated Logarithm Criterion (KLILC), among others (Dávila-Jiménez et al., 2014). The model selection depends on the sample size. The criteria estimate loss of information that a model records as a measure of distance from the true model (Alston et al., 2015). The SBIC and KLILC are usually used for large sample data while AIC are used for both large and small sample data. In the present work, only AIC are employed for both the adsorption isotherm and the kinetic studies.

Akaike information criteria

The *AIC* were developed by Akaike (1974). They are statistical tools that have been adopted for selecting the most fitted model amongst competing models with a varying number of parameters (Akpa and Unuabonah, 2011; Turner et al., 2015; Nayak and Pal, 2019). According to Nayak and Pal (2019), with the assumption of independent model errors and normal error distribution, the equation for using *AIC* is expressed as follows:

$$A_{IC} = 2N_p - N_e\, In\left(\frac{ERRSQ}{N_e}\right) \quad (62)$$

Sugiura (1978) and Hurvich and Tsai (1989) modified and advanced the model for a small data in which $(N_e/N_p) < 40$ as follows (Nayak and Pal, 2019):

$$(A_{IC})_{mod} = A_{IC} + \left[\frac{2N_p(N_p+1)}{N_e - N_p - 1}\right] \quad (63)$$

The use of Akaike weights, λ_i, and strength of evidence, *ER*, gives one greater insight into the relative merits of the competing models (Turner et al., 2015; Wagenmakers and Farrell, 2004; Ibrahim et al., 2018). The Akaike weight, λ_i, is expressed as:

$$\lambda_i = \frac{\exp(-0.5\Delta A_{IC})}{\sum_{k=1}^{n}\left[\exp - 0.5(\Delta A_{IC})_k\right]} \quad (64)$$

$$(\Delta A_{IC})_k = (A_{IC})_k - (A'_{IC})_k \quad (65)$$

$$ER = \frac{1}{\exp\left[-0.5(\Delta A_{IC})_k\right]} \quad (66)$$

where $(\Delta A_{IC})_k$ denotes the differences between the value of $(A_{IC})_k$ for the *kth* model and the minimum $(A_{IC})_k$ value of the best ranked model, denoted by $(\Delta A'_{IC})_k$.

Model selection criterion

The model selection criterion is a statistic that expresses a function for assessing competing models vying for the best fitted model and it is expressed as (Adekunbi et al., 2019):

$$MSC = In\left(\frac{ESS}{SSE}\right) - \frac{2P}{N} \quad (67)$$

$$ESS = \sum_{k=1}^{N_e}\left(Q_{k,pred} - \overline{Q}_{k,pred}\right)^2 \quad (68)$$

where *MSC* is the model selection criterion, *ESS* the sum of squares

Table 1. Mathematical expressions for error functions.

S/N	Error functions	Model	Reference
1	Coefficient of determination, R^2	$R^2 = 1 - \frac{\sum_{k=1}^{N_e}\left(Q_{k,expt} - Q_{k,pred}\right)^2}{\sum_{k=1}^{N_e}\left(Q_{k,pred} - Q_e\right)^2}$	Olafadehan (2021)
2	Average relative error, *ARE*	$ARE = \frac{100}{N_e}\sum_{k=1}^{N_e}\left\lvert\frac{Q_{k,expt} - Q_{k,pred}}{Q_{k,expt}}\right\rvert$	Chan et al. (2012)
3	Standard deviation of relative errors, *SRE*	$SRE = \sqrt{\frac{1}{N_e}\sum_{k=1}^{N_e}\left[\left(Q_{k,expt} - Q_{k,pred}\right) - ARE\right]^2}$	Popoola (2019)
4	Marquardt's percent standard deviation, *MPSD*	$MPSD = 100\sqrt{\frac{1}{N_e - N_p}\sum_{k=1}^{N_e}\left(1 - \frac{Q_{k,pred}}{Q_{k,expt}}\right)^2}$	Chan et al. (2012)
5	Normalized standard deviation, *NSD*	$NSD = 100\sqrt{\frac{1}{N_e - 1}\sum_{k=1}^{N_e}\left(\frac{Q_{k,expt} - Q_{k,pred}}{Q_{k,expt}}\right)^2}$	Ahmad et al. (2014)
6	Residual Root Mean Square Error, *RMSE*	$RMSE = \frac{1}{N_e - 2}\sqrt{\sum_{k=1}^{N_e}\left(Q_{k,expt} - Q_{k,pred}\right)^2}$	Alston et al. (2015)
7	Normalized chi-square test, χ^2	$\chi^2 = \sum_{k=1}^{N}\left[\frac{\left(Q_{k,expt} - Q_{k,pred}\right)^2}{Q_{k,expt}}\right]$	Amrhar et al. (2015a, b)
8	Sum of squares of the errors, *ERRSQ*	$ERRSQ = \frac{1}{N_e}\sum_{k=1}^{N_e}\left(Q_{k,expt} - Q_{k,pred}\right)^2$	Amrhar et al. (2015a, b)

Table 1. Contd.

9	Sum of absolute error, *EABS*	$EABS = \sum_{k=1}^{N_p} \left(Q_{k,expt} - Q_{k,pred}\right)$	Chan et al. (2012)
10	Hybrid functional error, *HYBRID*	$HYBRID = \frac{100}{N_e - N_p} \sum_{k=1}^{N_e} \left[\frac{\left(Q_{k,expt} - Q_{k,pred}\right)^2}{Q_{k,expt}} \right]$	Olafadehan (2021)

due to regression, that is, the sum of the squares of the difference of the predicted values and the mean value of the response variable and $\overline{Q}_{k,pred}$ is the mean of the predicted values.

Thermodynamics studies

The thermodynamic features and parameters (such as change in Gibbs free energy, ΔG^0, enthalpy change, ΔH^0, entropy change, ΔS^0) of the adsorption of methylene blue on chitosan flakes were determined using Equations 69 and 70 (Erdem et al., 2004; He et al., 2010; Hefni et al., 2019):

$$K_d = \left(\frac{c_0 - c_e}{c_e} \right) \times \frac{V}{M} \tag{69}$$

$$\Delta G^0 = \Delta H^0 - T\Delta S^0 = -RT\, In\, K_d \tag{70}$$

where K_d is the distribution coefficient (mL/g) and $c_d \left(= c_0 - c_e\right)$ the concentration of MB on chitosan flakes (mg/L). From Equation 70, the linear plot of $In\, K_d$ against T^{-1} enables ΔH^0 and ΔS^0 to be obtained from the slope $\left[= \left(-\Delta H^0 / R\right)\right]$ and intercept on vertical axis $\left[= \left(\Delta S^0 / R\right)\right]$, respectively.

The modified Arrhenius type equation is used to relate the sticking probability, S^*, to surface coverage, θ, thus (Najim et al., 2010):

$$S^* = (1-\theta)\exp\left(-\frac{E_a}{RT}\right) \tag{71}$$

Where

$$\theta = 1 - \frac{c_e}{c_0} \tag{72}$$

The linearized form of Equation 71 is given as:

$$In(1-\theta) = \frac{E_a}{RT} + In\, S^* \tag{73}$$

Hence, the linear plot of $In(1-\theta)$ against T^{-1} enables the activation energy, E_a, and S^* to be obtained from the slope and intercept on vertical axis, respectively.

RESULTS AND DISCUSSION

Characterization of chitosan flake

The physicochemical properties of the prepared chitosan flakes from *A. marginata* shell powder, which included moisture, ash, fiber and protein contents, average molecular weight and apparent viscosity, were reported in our recent work to be 5.5%, 0.25%, 2.70, (0.85 ± 0.27%), 220 kDa and (85.20 cP at 20°C), respectively (Bello and Olafadehan, 2021). Other properties of the chitosan flakes obtained in this study are particle size =150 µm, bulk density = 0.9 g/cm^3, pH = 7.3 and pHpzc = 7.8. Equally, the morphological features of the chitosan flakes were assessed using Scanning Electronic Morphology (SEM) at 10,000 and 11,000 magnifications in our investigation (Bello and Olafadehan, 2021). It was revealed in Bello and Olafadehan (2021) that the surfaces of the shell of *A. marginata* and the chitosan flakes possessed cavities, pores and rough surfaces, which are viable characteristics of a typical adsorbent such as chitosan flakes. Also, the Electron Dispersive X-ray Spectroscopy (EDS) spectrum and the distribution of chemical elements in the grated *A. marginata* shell waste revealed that the precursor contained the highest weight % of calcium (53.35) and least weight % of iron (0.52) with weight % of oxygen, silica, sodium, magnesium, phosphorus and carbon being 3.20, 1.72, 2.24, 3.32, 13.10 and 2.45, respectively (Bello and Olafadehan, 2021). The X-ray diffraction (XRD) of the prepared chitosan

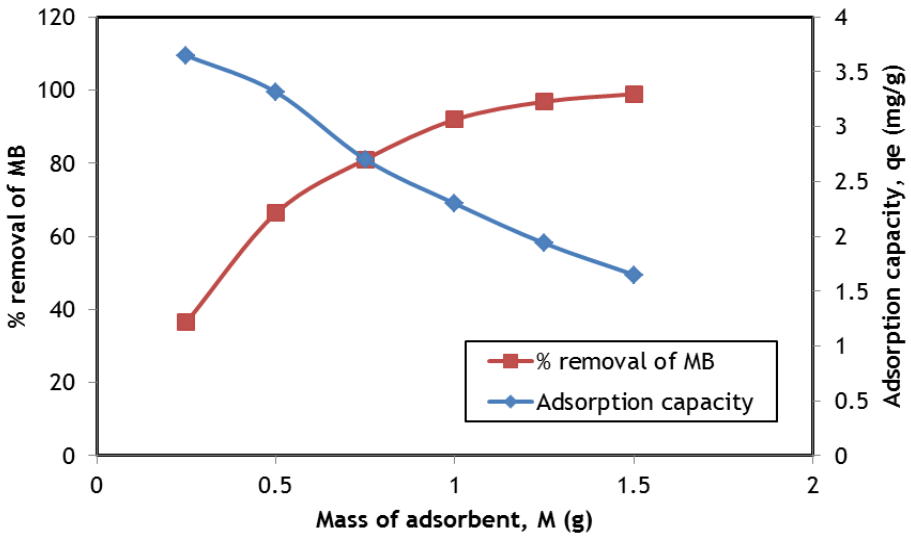

Figure 1. Effect of adsorbent dosage on removal efficiency and adsorption amount.

flakes indicated the crystalline natures of the biopolymer, where well-defined peaks, conspicuously among others at 2θ = 20 and 26°, were obtained (Bello and Olafadehan, 2021). In addition, the Fourier transform infrared spectroscopy (FT-IR) spectrophotometer (IS10, Thermo Nicolet, USA) in the wave number range of 4000-400 cm^{-1} with KBr pellet was used to determine the absorption bands and subsequent functional groups for *A. marginata* shell and the chitosan flakes before and after adsorption of methylene blue (Bello and Olafadehan, 2021). We showed that there was an interaction between methylene blue (MB) and the chitosan flakes and the adsorption was accomplished for reason of the significant differences in absorbance wavelength coupled with an increase in the absorbance wavelength of the amide and hydroxyl groups being responsible for the efficacious adsorption of methylene blue on the prepared chitosan flakes from *A. marginata* shell powder.

Effects of operational parameters on MB adsorption

Effect of adsorbent dosage

Figure 1 depicts the respective effects of the mass of adsorbent (chitosan flakes), *M*, on the removal efficiency of the chitosan flakes and the equilibrium adsorption capacity, q_e. It is revealed in the figure that the percentage removal of MB increases appreciably with increase in adsorbent mass owing to the fact that an increase in adsorbent mass leads to an increase in the number of active sites, except for cases of overlapping of adsorption sites or due to the screening effect occasioned by overcrowding of adsorbent where the percentage removal of the target pollutant shows no further increase (Benzaoui et al., 2018).

It was observed in Figure 1 that the adsorption capacity decreases with a corresponding increase in the dosage of the adsorbent. This is as a result of entire exposure of the actives sites at low amount of adsorbent dose while a few fractions were exposed at higher dose of the chitosan flakes (Alghamdi et al., 2019).

Effect of solution pH

The influence of pH of methylene blue solution on adsorption capacity, q_e, of the chitosan flakes and % removal of MB was investigated by varying the solution pH values for an initial concentration of MB of 100 mg/L at 303 K. Figure 2 reveals that the pH of solution influences appreciably the percentage of MB molecules adsorbed on the chitosan flakes and the adsorption capacity of the chitosan flakes within a pH range of 2 to 12 considered. The percentage removal of MB increases from 49.82 to 98.95 at solution pHs of 2.4 and 11.8, respectively largely due to the pH of zero point charge (pHzpc) of the adsorbent measured at 7.3. At a solution pH lower than zero-point charge $\left(pH < pH_{zpc}\right)$, the surface charge of the adsorbent becomes positively charged and initiates the presence of hydrogen ions, which heightened the competition between the MB cations and the hydrogen ions on the active site of the adsorbent. Thus, % removal of MB as well as the adsorption capacity is low. Conversely, at higher solution pH, the surface charge of the adsorbent becomes negatively charged owing to the large presence of hydroxyl ions, which eventually paved way for less competition and facilitates the electrostatic forces of attraction between the cations of MB on the much available actives sites (Bernal et al., 2017; Boumediene

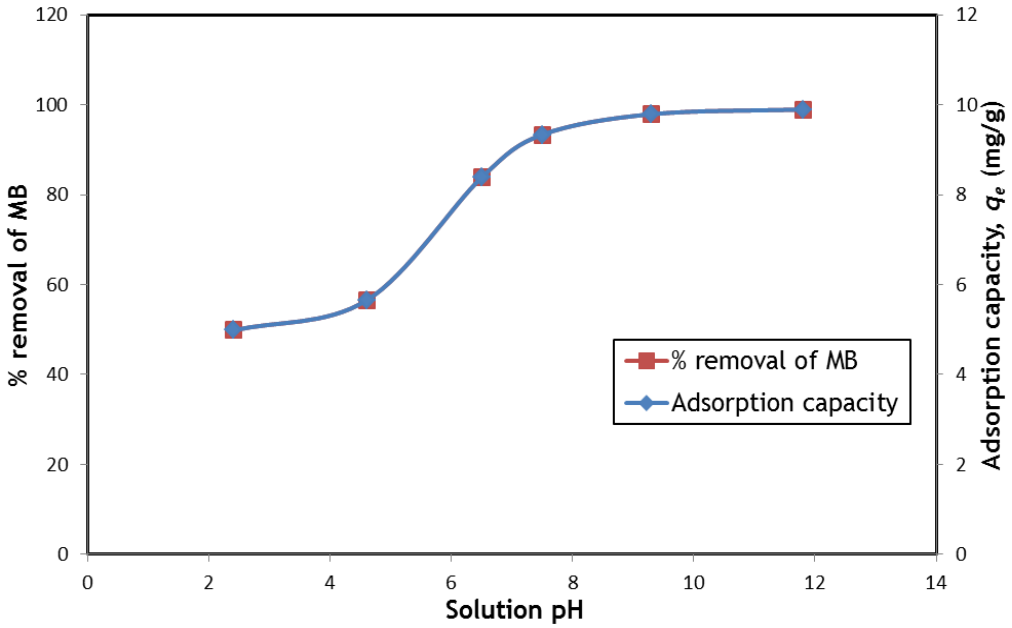

Figure 2. Effect of solution pH on removal of MB on chitosan flakes and adsorption capacity.

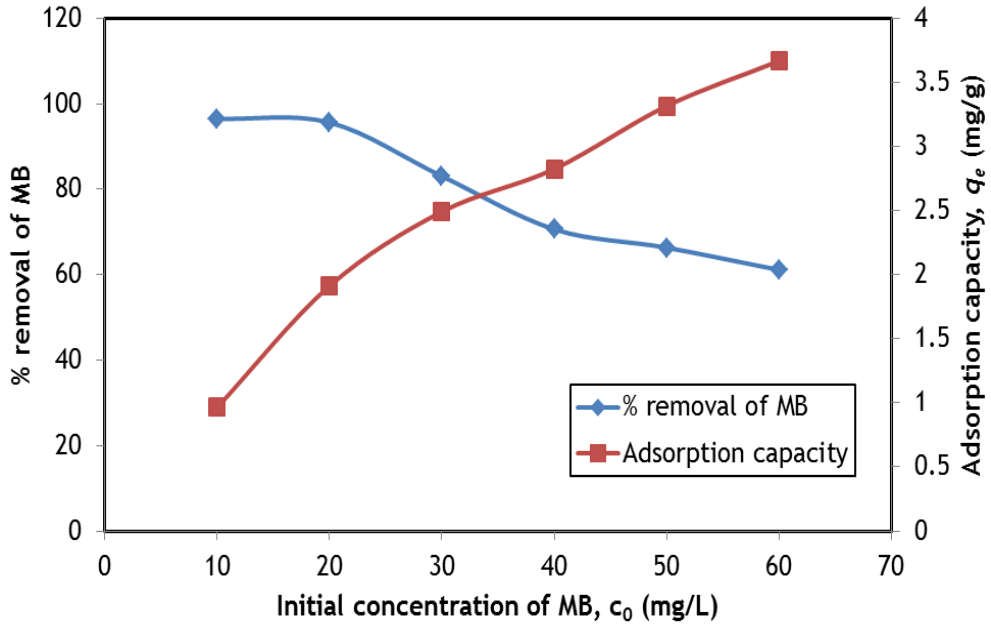

Figure 3. Effect of initial concentration of MB on adsorption capacity and % removal of MB.

et al., 2018). Thus, a relatively high amount of MB adsorbed on the chitosan flakes as well as adsorption capacity was achieved.

Effect of initial MB concentration

The respective effects of the initial methylene blue concentrations on the % removal of MB and adsorption capacity of the chitosan flakes were shown in Figure 3. The percentage removal of MB decreases from 96.49 to 61.11 as the initial concentration of MB increases from 10to 60 mg/L while the amount of MB adsorbed per unit mass of chitosan flakes increases significantly from 0.9641 to 3.67 mg/L as the initial MB concentration increases from 10 to 60 mg/L as a result of the

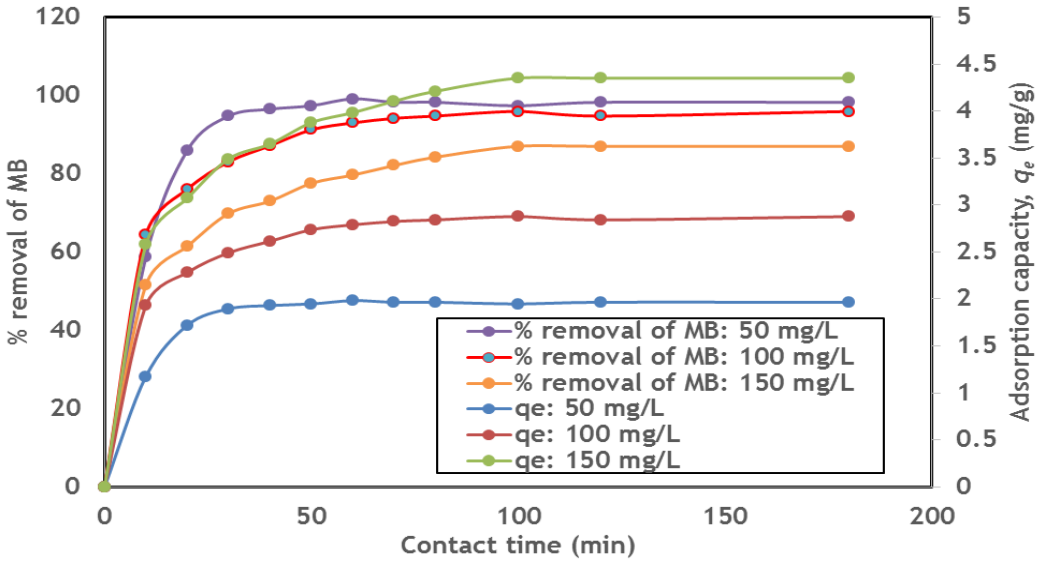

Figure 4. Effect of contact time on the adsorption amount and removal efficiency of MB using chitosan flakes at pH = 8.2, adsorbent dose of 0.1 g and varying initial concentrations, c_0, of 50, 100 and 150 mg/L.

unavailable requisite number of active sites to cater for the increased initial concentration of MB (Edet and Ifelebuegu, 2020).

Effect of contact time

The contact time is an influential factor and a key parameter for design, management and operation of wastewater treatment. Figure 4 shows the amount of MB adsorbed per unit mass of chitosan flakes and percentage removal of MB against contact time at a temperature of 30°C, pH of 8.2, adsorbent dose of 0.1 g and varying initial MB concentrations, c_0, of 50 mg, 100 mg/L and 150 mg/L. It was observed that the first phase of adsorption of MB on the chitosan flakes, which is characterized by a steeper gradient, depicts an increment in the percentage removal of MB and the amount of MB adsorbed per unit mass of the chitosan flakes as the contact time increases until the second phase, which is recognized as the equilibrium stage, was attained. During the first phase, the enormous number of vacant active sites is available for the adsorption of MB molecules on the chitosan flakes. However, at the second stage in the adsorption process characterized with a plateau, there are no significant observable changes in both the % removal of MB and the adsorption capacity of the chitosan flakes due to the few available sites and possible repulsive forces between MB molecules adsorbed on the chitosan flakes and the solution phase ((Edet and Ifelebuegu, 2020; Slimani et al., 2011). Equilibrium times were established at 70, 80 and 100 min with % removal of MB of 98.2, 94.7 and 87 at initial concentrations of MB of 50, 100 and 150 mg/L respectively. In a similar fashion, the amount of MB molecules adsorbed per unit mass of the chitosan flakes at the respective established equilibrium times was obtained as 1.96, 2.84 and 4.35 mg/g for 50, 100 and 150 mg/L. These results imply that the higher the initial concentration of MB, the higher the equilibrium time and conversely (Kuang et al., 2020).

Effect of temperature

The respective effects of temperature on the percentage adsorption of MB ions and the adsorption capacity of the chitosan flakes are depicted in Figure 5. It was observed that the percentage removal of MB and adsorption capacity of the chitosan flakes reduce as the temperature increases. These obvious trends lend credence to the fact that the adsorption process is favored at low temperature and inimical at high temperature. From literature, this equally inferred that the process of adsorption is an exothermic one, which is in consonance with the thermodynamics parameters estimated (Edet and Ifelebuegu, 2020; Horsfall and Spiff, 2005).

Analysis of 2-p adsorption isotherms

The Gill isotherm classification enables an insight to the specific adsorption process. Figure 6 shows the relationship between q_e and c_e, wherein an “L” shape is

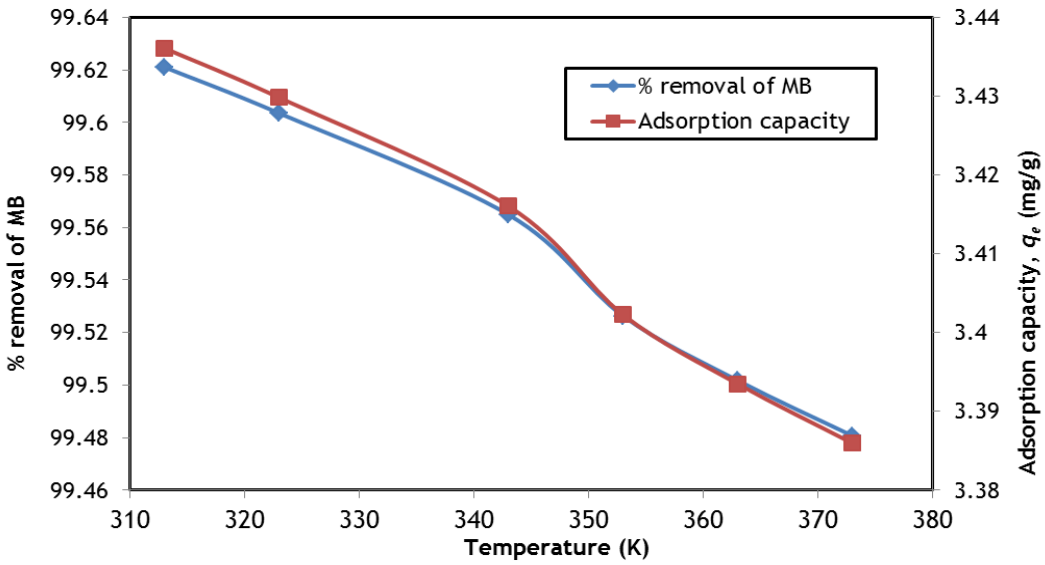

Figure 5. Effect of temperature on adsorption capacity and % removal of MB.

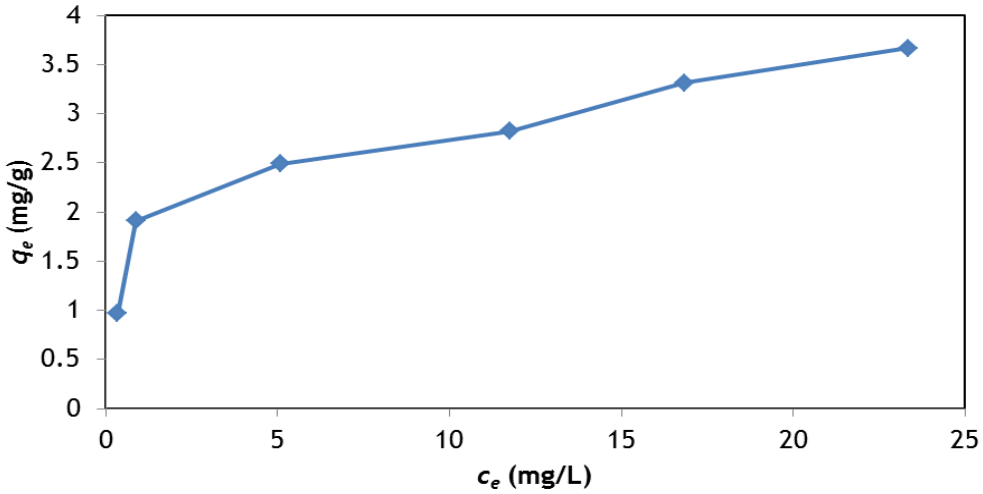

Figure 6. q_e against C_e.

obtained. This implies that there is no strong competition between the solvent and the adsorbate vying for the occupation of the adsorbent surface sites. It can equally be inferred that the methylene blue molecules are adsorbed flat on the surface of the chitosan flakes because the longitudinal axes of the adsorbed MB molecules are parallel to the adsorbent surface (Hamdaoui and Naffrechoux, 2007).

All the isotherms investigated in this study were attempted to be fitted to the batch equilibrium data of MB adsorption on chitosan flakes as adsorbent at pH=8.2, temperature of 30°C, agitation speed=150 rpm and adsorbent dose of 0.1 g.

From the linear plot of 2-p Freundlich isotherm, expressed in Equation 2, the estimated R^2 value is 0.914, the adsorption intensity, *N*, is 3.663 and the measure of adsorption capacity, k_F = 1.5516. The calculated value of $1/N$ (= 0.273) is within the range of 0.1 to 1.0. Thus, the adsorption of MB on the prepared chitosan flakes is adjudged to be a good adsorption process (Kuang et al., 2020). From the literature, it was reported that adsorption process is good for $2 \le N < 10$, moderate difficult for $1 \le N < 2$ and poor for $N < 1$ (Olafadehan et al., 2018; Razavi et al., 2013; Húmpola et al., 2013; Chen et al., 2010; Tahir and Rauf, 2006). Hence, the 2-p Freundlich isotherm obtained for the

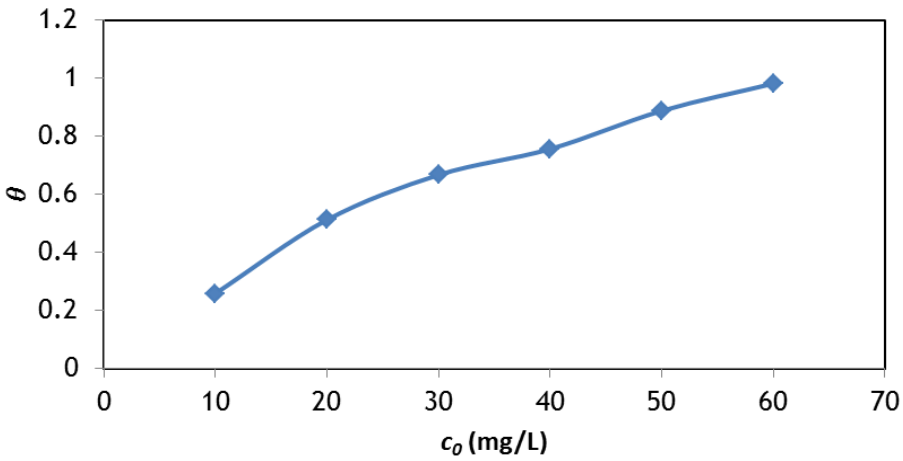

Figure 7. Surface coverage against initial concentration of methylene blue.

removal of MB using chitosan flakes from *A. marginata* shell powder is given by $q_e = 1.5516 c_e^{0.273}$.

From the linear plot of 2-p Langmuir isotherm, expressed in Equation 4, q_{max} and K_L were obtained to be 3.7327 mg/g and 0.5615 L/mg, respectively with the coefficient of determination, R^2 = 0.9816, which gives an impression of a better fit to the adsorption of MB on chitosan flakes than the 2-p Freundlich isotherm. The essential attributes of the model regarded as separation factor, R_L, was evaluated to be in the range $0 < R_L < 1$ for c_0 = 10 to 60 mg/L. Hence, the adsorption process is adjudged to be favorable. Figure **7** shows the variation of surface coverage, θ, with initial concentration, c_0, of methylene blue solution. It is revealed that a rapid succession of chitosan flakes surface coverage fraction increases as the initial concentration of MB increases till θ is close to unity, which is in consonance with the underlying assumptions of Langmuir isotherm.

From the linear plot of 2-p Temkin isotherm, expressed in Equation 6, the isotherm constants, b_T and A_T were evaluated to be 4481.6616 J/mol and 20.4606 L/h respectively with the coefficient of determination, R^2=0.9533, which gives an impression of a better fit to the adsorption data of MB on chitosan flakes than the 2-p Freundlich isotherm but otherwise for the 2-p Langmuir isotherm. The positive value of b_T, which is related to the variation of the adsorption energy, indicated that the adsorption process was endothermic (Ghogomu et al., 2013; Inam et al., 2016).

From the linear plot of the 2-p Dubinin-Radushkevish isotherm, expressed in Equation 8, the isotherm constants, β and q_{DR} were evaluated to be 1.0×10^{-7} $(mol/J)^2$ and 3.0213 mg/g respectively with R^2 = 0.9254. The mean energy of adsorption, *E* was calculated to be 2.2361 kJ/mol. From the literature, the mean energy of adsorption value indicates physical adsorption for values of 1–8 kJ/mol; ion-exchange for values of 8-16 kJ/mol and 20-40 kJ/mol for chemisorption (Chen et al., 2010; Tahir and Rauf, 2006). This result clearly reflects a physical adsorption process of MB adsorption on chitosan flakes from *A. marginata* shell powder.

From the linear plot of 2-p Harkins-Jura isotherm, expressed in Equation 12, the isotherm constants, A_{HJ} and B_{HJ} were evaluated to be 2.2894 and 1.3299 g/mg^2, respectively with a relatively poor regression coefficient, R^2=0.7044.

From the linear plot of 2-p Frenkel-Halsey-Hill isotherm, expressed in Equation (14), the isotherm constants, n_{FHH} and K_{FHH} were evaluated to be -3.6630 and 0.2, respectively with regression coefficient, R^2=0.914.

From the linear plot of 2-p Brunauer-Emmett-Teller isotherm, expressed in Equation 16, which is designated as BET1 isotherm in this study, the isotherm constants, q_S and c_{BET} were evaluated to be 99.99 mg/L and 1.00, respectively with a significant high regression coefficient, R^2=0.9816 for the saturated concentration, c_S, of MB used = 43210 mg/L (Salimi and Roosta, 2019).

The estimated parameter values of the 2-p isotherms using linear regression methods are shown in Table 2.

The decreasing order of the fit of the isotherms to the equilibrium adsorption data of MB on chitosan flakes, as shown in Table 2, is 2-p Langmuir isotherm, 2-p BET1 isotherm > 2-p Temkin isotherm > 2-p Dubinin-Radushkevish isotherm > 2-p Frenkel-Halsey-Hill isotherm > 2-p Harkins-Jura isotherm, 2-p Freundlich isotherm. Hence, 2-p Langmuir and 2-p BET1 isotherms are adjudged to correlate best the adsorption of MB on chitosan flakes.

Table 2. Comparison of linear and non-linear adsorption isotherm parameters.

Isotherm	Parameter	Estimated values using linear form	Estimated values using non-linear form
2-p Freundlich	N	3.6630	1.6310
	k_f (mg/g)	1.5516	3.9800
	R^2	0.9140	1.0
2-p Langmuir	q_{max} (mg/g)	3.7327	3.4824
	K_L (L/mg)	0.5615	1.1818
	R^2	0.9816	1.0
	R_L	$0<R_L<1$	$0<R_L<1$
2-p Temkin	b_T (J/mol)	4481.6616	4439.68
	A_T (L/g)	20.4606	20.4870
	R^2	0.9533	1.0
2-p Dubinin-Radushkevish	β (mol/J)^2	1.0×10^{-7}	7.0×10^{-8}
	q_{DR} (mg/g)	3.0213	3.3109
	R^2	0.9254	0.8331
	E (kJ/mol)	2.2361	2.6726
2-p Harkins-Jura	A_{HJ}	2.2894	2.3008
	B_{HJ} (g/mg)^2	1.3299	1.7079
	R^2	0.7044	1.0
2-p Frenkel-Halsey-Hill	n_{FHH}	-3.6630	-3.9763
	K_{FHH}	0.2	0.1433
	R^2	0.914	1.0
2-p BET1	q_S (mg/L)	99.99	3.6313
	c_{BET}	1.00	26832
	R^2	0.9816	1.0

Analysis of adsorption isotherms using non-linear regression analysis

For the purpose of adequate modeling of the adsorption process of MB on chitosan flakes and to evaluate the affinity of MB on the chitosan flakes, nineteen different adsorption isotherms were investigated using non-linear method characterized by trial-and error-procedure aided by the SOLVER ADD-IN obtained in MICROSOFT EXCEL SPREADSHEET and guided by 9 different error functions aside the R^2 function shown in Table 1. These involve seven two-parameter isotherms, eight three-parameter isotherms, three four-parameter and one five-parameter isotherms. The algorithm adopted in this work for non-linear evaluation of isotherm and kinetic models' parameters is the one given by Popoola (2019) with slight modification of the inclusion of statistical evaluation as another criterion for model selection amongst competing models and the process for evaluating sum of normalized errors (SNE) adopted for the isotherm and kinetic models' parameters is given by Amrhar et al. (2015a, b).

The estimated parameter values of the 3-p, 4-p and 5-p isotherms using non-linear regression methods are summarized in Table 3.

Table 3. Values of three, four and five-parameter isotherms using non-linear method.

Isotherm	Parameter	Estimated value using non-linear method
3-p BET2	q_s	2.6489
	c_{BET}	160.5411
	c_s	77.0698
	R^2	1.0
3-p BET3	q_m	2.6496
	K_s	2.0696
	K_L	0.0130
	R^2	1.0
3-p Redlich-Peterson	k_{RP}	11.7778
	α_{RP}	6.0082
	β_{RP}	0.8079
	R^2	1.0
3-p Toth	q_m	3.4824
	K_T	1.1818
	β_T	1.0
	R^2	0.9149
3-p Sips	q_{SP}	14.4412
	K_{SP}	0.1277
	β_S	3.3306
	R^2	1.0
3-Khan	q_{max}	1.3364
	b_K	6.1178
	a_K	0.8023
	R^2	1.0
3-p Radke-Prausnitz	q_{max}	1.3363
	K_{RPI}	6.1174
	α_{RPI}	0.8023
	R^2	1.0

Table 3. Contd.

3-p Fritz-Schlüender	$(q_m)_{FS}$	6.0236
	K_{FS}	1.9582
	α_{FS}	0.8075
	R^2	1.0
4-p Fritz-Schlüender	A_{FS}	4.8087
	Φ_{FS}	1.5489
	B_{FS}	3.1480
	β_{FS}	0.8541
	R^2	1.0
4-p Bauder	$(q_m)_B$	2.0254
	b_0	1190.71
	x	5.3247
	y	0.1884
	R^2	1.0
4-p Marczewski-Jaroniec	$(q_m)_{MJ}$	4.3910
	K_{MJ}	0.02
	α_{MJ}	6.3960
	β_{MJ}	0.2410
	R^2	1.0
5-p Fritz-Schlüender	$(q_m)_{FS5}$	143.6660
	K_{FS5}	3.9303
	α_{FS5}	0.2060
	Φ_{FS5}	306.3960
	β_{FS5}	0.00035
	R^2	1.0

A closer examination of the results in Tables 2 and 3 depicts that the non-linear method gives the better fit of the isotherms to the adsorption data of MB on chitosan flakes than the linear method on the basis of high regression coefficient, R^2, which almost gave a value of 1 in all cases, except for 2-p Dubinin-Radushkevich and 3-p Toth isotherms with R^2 values of 0.8331 and 0.9149, respectively.

Kinetic study

Linearized kinetic models

The necessary linear plot for each of the adsorption kinetics investigated in the current study for the adsorption of MB on chitosan flakes was made to

determine the kinetic parameters inherent in it. Table 4 presents the values of the kinetic parameters in each of the 8 kinetic models investigated for the adsorption of MB on chitosan flakes using the linearized kinetic models.

For the fractional power kinetic model, the exponent, v, at all initial MB concentrations was found to be less than unity with a good correlation value at initial methylene blue concentrations of 100 and 150 mg/L shown in Table 4. This validates the time-dependence behavior during the adsorption of MB on the chitosan flakes (El-Khaiary and Malash, 2011).

At concentrations of MB of 50, 100 and 150 mg/L initially, high regression coefficients, R^2, of 0.9529, 0.9726 and 0.9894 were obtained respectively using the Lagergren pseudo first-order kinetic model. As presented in Table 4, higher values of regression coefficient were marginally obtained for the pseudo second-order kinetic model than for the Lagergren pseudo first-order kinetic model and any other kinetic models at all the initial concentrations of MB investigated. It was thus observed that R^2 values of 0.9924, 0.9996, 0.9984 at initial MB concentrations of 50, 100 and 150 mg/L, respectively are good representations of the experimental kinetic data of MB adsorption on chitosan flakes.

In Table 4, the Elovich kinetic model equally gave high regression coefficient values, which are good enough to fit the experimental kinetic data of the adsorption of MB on chitosan flakes but not as high as the R^2 values obtained using the pseudo second-order model.

For the intra-particle diffusion (IPD) model, reasonably good R^2 values were obtained, with straight line not passing through the origin at all initial concentrations of MB considered, as shown in Figure 8. Consequently, the intraparticle diffusion was not the rate-limiting step in the adsorption of MB on the chitosan flakes. The plots of the model had intercepts for all initial concentrations of MB of 50, 100 and 150 mg/L. The value of the intercept increases significantly with initial MB concentrations of 50 to 100 mg/L and then decreases slightly at 150 mg/L. This gives the impression that the boundary layer linked to the intercepts may likely increase with increase in initial concentrations of MB in the range 50 to 100 mg/L.

A closer observation of the graphs in Figure 8 shows a multi-linear one of three distinct phases, especially for the initial concentrations of MB solution under study. The first phase was observed to be relatively fast due to boundary layer or strong electrostatic attraction of MB on the external surface of the chitosan flakes. The second observable phase is a palpable gradual adsorption stage suggested to be influenced or occasioned by intraparticle as the rate-limiting step at this stage, which culminated to the equilibrium phase (that is, the third phase) with high affinity to the chitosan flakes surface active sites (Zbair et al., 2018).

The estimated intra-particle diffusion rate constant, k_{IPD}, shows a gradually retrogression from the slopes values of the multi-lines under study. The intercept values, *C*, for each observed stage shows progressive increment in value as the initial concentration of MB increases. This presupposes the boundary effect is taking a toll on the adsorption process. Such increase in boundary layer thickness would pave way for low external mass transfer and high chances of internal mass transfer.

The Boyd model plot in Figure 9 confirms that the intra-particle diffusion step is not the rate-controlling step in the adsorption of MB on chitosan flakes but rather film diffusion (external diffusion) due to the linearity observed to be away from the origin.

In Table 4, the diffusion-chemisorption model equally gave high regression coefficient values, which are good enough to fit the experimental kinetic data but not as high as the pseudo second-order model. Using the diffusion-chemisorption model, the resulting straight line, coupled with high regression coefficient values, shows that the sorption process is under the influences of both diffusion and chemisorption.

Results from non-linear kinetic model

The estimated kinetic parameters for the non-linea kinetic models using non-linear regression method subjected to the error functions used previously are shown in Table 5. Using the values of the coefficient of determination, the non-linear method gave a better fit than the linear method. With the various error functions employed, for MB concentration of 150 mg/L, *NSD* function fitted 4 kinetic models (fractional power model, pseudo second-order model, Elovich model, intraparticle diffusion, IPD (or Weber-Morris) model); *EABS* fitted 1 model (Lagergren pseudo first-order model); *ARE* fitted 1 model (Avrami model) and *RSME* fitted 1 model (diffusion-chemisorption model). For MB concentration of 100 mg/L, *NSD* fitted 4 models (fractional power model, Lagergren pseudo first-order, Elovich and IPD models); *ARE* fitted 1 model (pseudo second-order model); *RSME* fitted the diffusion-chemisorption model and *HYBRID* function fitted 1 model (Elovich model). For the case of initial concentration of MB of 50 mg/L, *NSD* function fitted 3 models (Lagergren pseudo first-order, pseudo second-order and Elovich models); *SSE* fitted 1 model (IPD model); *HYBRID* fitted 1 model (Avrami model); *RSME* fitted 1 model (fractional power law) and *SRE* function fitted 1 model (diffusion-chemisorption model).

Isotherm and kinetic models' selection

Since the sum of normalized error (*SNE*) has been reported as a way or criterion for selecting the best fitted isotherm/kinetic model (Anirudhan and Radhakrishnan, 2009; Yanev et al., 2013; Popoola, 2019), the *SNE* value was used as a yardstick for the model selection in this

Table 4. Values of the parameters in the linearized kinetic models for the adsorption of MB on chitosan flakes.

Kinetic model	Parameter	Values of the parameters at initial MB concentration		
		50 mg/L	100 mg/L	150 mg/L
Fractional power	v	0.135	0.1637	0.2363
	k_f	1.1632	1.6900	1.5186
	R^2	0.8760	0.9873	0.9918
Lagergren pseudo first-order kinetic model	k_1 (min^{-1})	0.0788	0.0635	0.0345
	q_e (mg/g)	1.3620	2.150	2.5870
	R^2	0.9529	0.9726	0.9894
Pseudo second-order kinetic model	k_2 (g/(mg min))	0.0550	0.0520	0.0220
	q_e (mg/g)	2.3030	3.5740	4.6707
	h (mg/(g min))	0.2917	0.6642	0.4799
	R^2	0.9924	0.9996	0.9984
Elovich kinetic model	α (mg/(g min))	0.5224	8.5724	0.6032
	β (g/mg)	2.0593	2.1240	0.7955
	R^2	0.9941	0.9970	0.9029
Avrami kinetic model	n_{AV}	0.3300	-0.7476	-0.6277
	k_{AV} ($\min^{-n_{AV}}$)	1.0932	0.1825	0.1956
	t_a (min)	0.7722	0.1040	0.0752
	R^2	0.9942	0.9592	0.9776
Intraparticle diffusion (IPD)	k_{IPD} (mg/(g $min^{½}$))	0.1914	0.1710	0.2773
	C (mg/g)	0.7186	1.9826	2.8335
	R^2	0.8226	0.9558	0.9724
Boyd model	D (m^2/s)	4.4911×10^{-11}	3.6191×10^{-11}	1.9663×10^{-11}
	R^2	0.9529	0.9726	0.9893
Diffusion-chemisorption model	k_{DC} (mg/(g $min^{-0.5}$))	1.2979	1.7550	1.3419
	q_e (mg/g)	2.5100	4.330	6.4800
	k_i (mg/(g min))	0.6711	0.7113	0.2779
	R^2	0.9865	0.9994	0.9980

study. The most fitted model amongst the non-linearized isotherms using the non-linear regression method is the one with the lowest value of *SNE*. The computed *SNE* values for the2-p isotherms, 3-p isotherms, 4-p isotherms

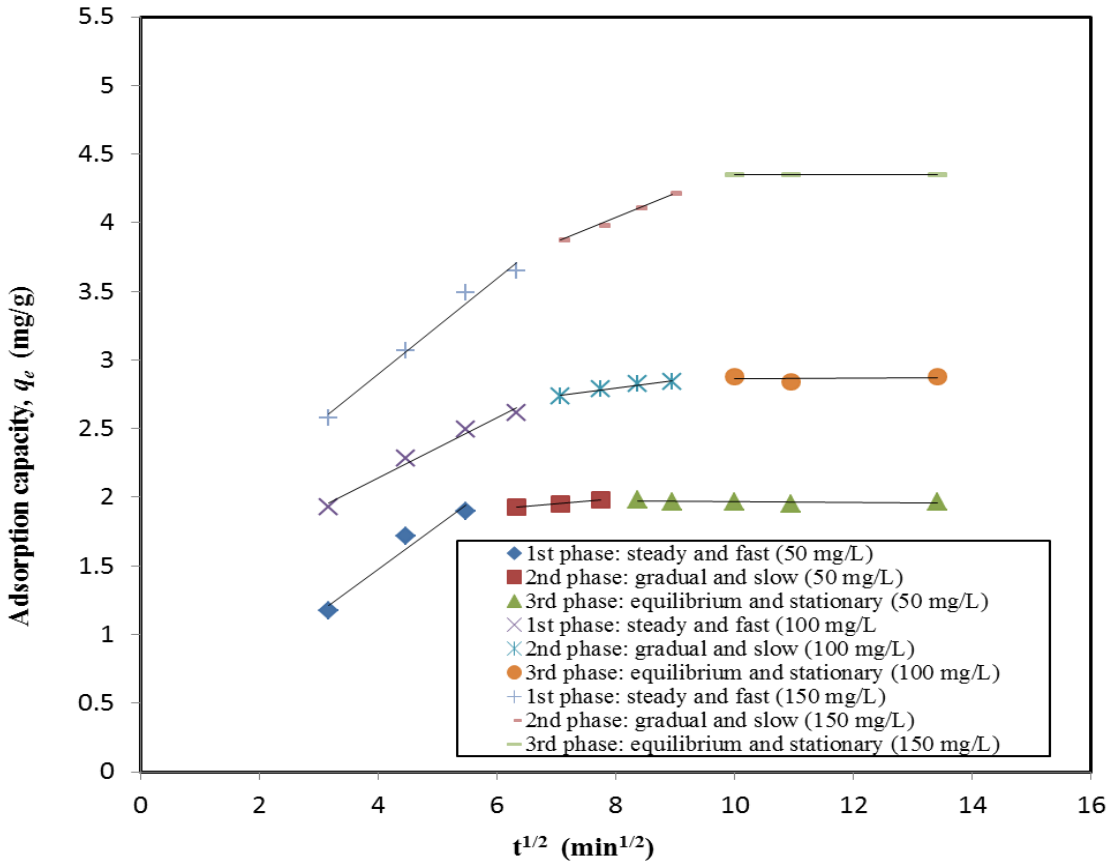

Figure 8. Variation of adsorption amount at any time *t* against *t* for intra-particle diffusion (IPD) model: mass=0.1 g; pH=8.2; agitation speed=150 rpm and temperature=30^{o}C.

and 5-p isotherm are shown in Table 6. The 5-p Fritz-Schlüender isotherm gave the lowest *SNE* value closely followed by the 2-p Temkin isotherm. Thus, the former is the most fitted isotherm using the *SNE* value as selection. Moreover, the lowest values of Pearson's chi-squared analysis, Akaike information criterion (*AIC*), model selection criterion for isotherm models and its associated values for each of the isotherm models investigated are shown in Table 6. Using the *SNE* for the goodness-of-fit amongst the two-parameter isotherms considered, the 2-p Temkin isotherm fitted best the adsorption equlibrium data of MB on chitosan flakes having a value of 4.7721 with the *NSD* stastistical indicator. For the three-parameter isotherms, Redlish-Peterson isotherm fitted best, which recoded a value of 5.0828 with *EABS* as error function while Marczewiski-Jaroniec isotherm fitted best amongst the four-parameter isotherms having a value of 6.2345 with *MPSD* as error function. The 5-p Fritz-Schlüender isotherm fitted best overall among all other number of parameters of the isotherm considered having the least value of 4.6506 with the *NSD* error function. The lowest value of *SNE* with the corresponding error function reflect the optimum isotherm parameter for the various isotherm models considered (Ghaffari et al., 2017; Rahman et al., 2018). In all the 19 isotherm models considered, *NSD* best fitted for 12 adsorption isotherms, chi-squared best fitted for 4 isotherms while *MPSD*, *EABS* and *HYBRID* best fitted for 1 isotherm each. Also from Table 6, the Pearson's Chi-squared $\left(\chi^2\right)$ analysis carried out at the respective degree of freedom, *df*, (difference between the number of experimental data and the number of parameters) shows that all the models have a non-significant lack of normality of the residuals since the calculated value is less than the critical or table value. Statistically, it translates or reveals a high level of acceptance of the models (Mitrevski et al., 2017). In addition, the results projects Bauder isotherm as the best fitted isotherm in terms of normality of residual followed by the 3-p BET2 and 3-p BET3 isotherms in descending order.

The *AIC* function is a statistical tool well rootedas a yardstick for comparing model equations with varying number of parameters. Its principle of operation is hinged simply on the difference between calculated *AIC* values over a set of model equation with a likely product of positive or negative value. The $\left(A_{IC}\right)_{mod}$ value of a model equation with the lowest value (considering the sign),

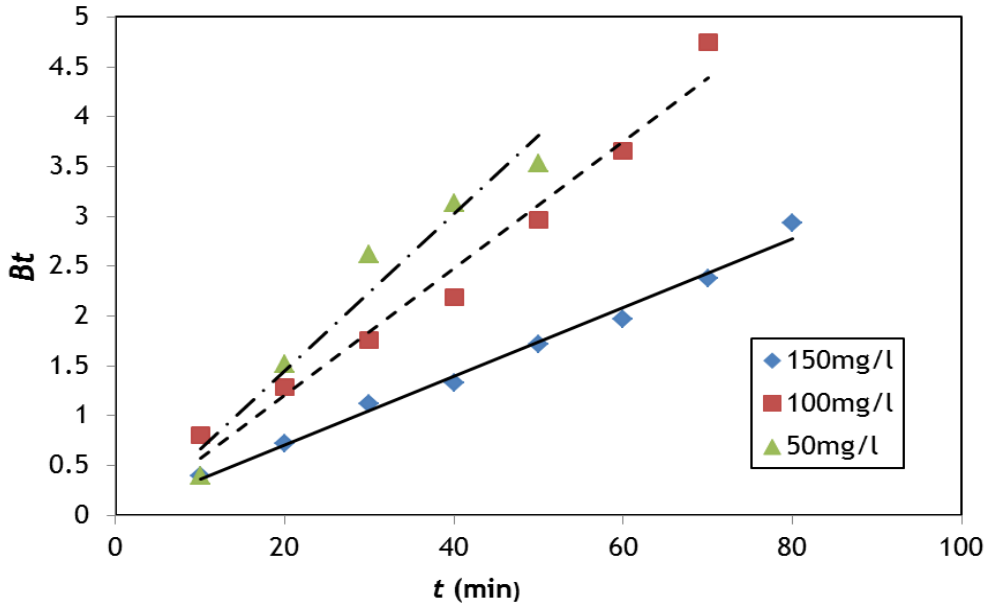

Figure 9. Boyd plot for the adsorption of MB on chitosan flakes.

lowest value of evidence ratio (*ER*) and the highest value of model selection criterion (*MSC*) amongst the competing equations is adjudged to be the superior equation over others (Akaike, 1974). From the results in Table 6, the 3-p BET2 and 3-p BET3 model equations portrayed the same lowest value of $(A_{IC})_{mod}$ = -16.2878 and evidence ratio, *ER*, of 1. With the highest value obtained for *MSC*, the 3-p BET3 isotherm is considered the most fitted model for the adsorption of MB on the synthesized chitosan flakes.

Similarly, using the information-based criteria for the selection of the best fitted kinetic models for the adsorption of MB on chitosan flakes, the pseudo second-order kinetics recorded the lowest $(A_{IC})_{mod}$, lowest evidence ratio and highest *MSC* values, amongst all the investigated kinetic models, at all initial concentrations of MB solution under this present study, as revealed in Tables 7 and 8. Hence, the adsorption rate of MB on chitosan flakes can be kinetically described by the pseudo second-order model, with the model satisfying all the criterial used in selecting the best fitted kinetic models.

In the same vein, the Pearson's chi-squared analysis carried out at the respective degree of freedom shows that all the models have a non-significant lack of normality of the residuals. The same trend was observed in all the criteria as shown in the ranking for the best fitted kinetic models.

Thermodynamics study

The effect of temperature in adsorption studies is considered as a fundamental factor in adsorption systems. It gives the thermodynamics parameters: activation energy, sticking probability and changes in entropy, enthalpy and Gibbs free energy. From the results in Table 9 and Figure 10, ΔH^0 is positive, which indicates an endothermic process of adsorption of MB on the prepared chitosan flakes from *A. marginata*. This implies that adsorption capacity of the derived chitosan flakes increases with temperature.

The value of ΔH^0 is within the range of 1-8 kJ/mol for physisorption (Zarrouk et al., 2011). Also, the positive value of ΔS^0 suggests a high degree of randomness at the chitosan-MB interface with appreciable structural changes with the adsorbate species (Saha and Chowdhury, 2011). It is also noteworthy that the negative value of the Gibbs free energy, ΔG^0, reflects a high degree of spontaneity of the adsorption process of MB on chitosan flakes and exergonic and energetically favorable adsorption process with increasing negative values occasioned by increases in temperature.

The sticking probability, S^*, known as the rate of adsorption per molecular collision with the adsorbent surface, directly expresses the difficulty encountered by a molecule in overcoming the barrier to adsorption. The calculated value of S^*, which is less than unity, indicates that the likelihood of MB ions sticking onto the chitosan surface is very high.

Batch reactor design

Figure 11 illustrates briefly the batch reactor design using

Table 5. Estimated values of the parameters in the non-linear kinetic models for the adsorption of MB on chitosan flakes using non-linear regression method.

Kinetic model	Parameter	Values of the parameters at initial MB concentration		
		50 mg/L	100 mg/L	150 mg/L
Fractional power	v	0.1095	0.1360	0.2018
	k_f	1.2886	1.5827	1.7335
	R^2	1.0	1.0	1.0
Lagergren pseudo first-order kinetic model	k_1 (min^{-1})	0.1065	0.0774	0.0910
	$(q_e)_{expt}$ (mg/g)	1.9649	2.8420	4.3509
	q_e (mg/g)	1.9575	2.7381	3.7477
	R^2	1.0	1.0	1.0
Pseudo second-order kinetic model	k_2 (g/(mg min))	0.0602	0.0287	0.0559
	q_e (mg/g)	2.2813	3.3044	4.0516
	h (mg/(g min))	0.3133	0.3134	0.9176
	R^2	1.0	1.0	1.0
Elovich kinetic model	α (mg/(g min))	3.9943	2.2664	1.4534
	β (g/mg)	13.9360	4.1265	3.4587
	R^2	1.0	1.0	1.0
Avrami kinetic model	n_{AV}	4.0761	4.0761	4.0761
	k_{AV} ($\min^{-n_{AV}}$)	2.7060	2.7060	2.7060
	q_e (mg/g)	1.9298	2.614035	3.6491
	t_a (min)	0.7924	0.7924	0.7924
	R^2	0.8534	0.8610	0.8315
Diffusion-chemisorption model	k_{DC} (mg/(g $min^{-0.5}$))	0.0990	0.2100	0.5
	q_e (mg/g)			
	k_i (mg/(g min))	0.0040	0.01432	0.0612
	R^2	1.0	1.0	1.0

Equation 35. The plots so obtained shows the mass of chitosan flakes to increase with increasing solution volume at a certain % removal of MB using the chitosan flakes prepared from *A. marginata* shell waste.

Proposed adsorption mechanism of methylene blue onto chitosan flakes

The reaction mechanism of the adsorption of MB onto chitosan (CH) was proposed by noting that the adsorption mechanism is dependent on the electrostatic attractive force between the surface of the chitosan (biosorbent) and the methylene blue, which are negatively and positively charged respectively. The electrostatic force of attraction arises as a result of the functional groups present on the surface of the chitosan and the pH dependence of MB adsorption from aqueous solution onto the chitosan flakes. The presence of hydroxyl (OH^-) and amide (NH_2^-) groups on CH was revealed

Table 6. Results of SNE, Pearson's chi-squared analysis, Akaike information criterion (AIC) and model selection criterion for isotherm models.

Isotherm	N_p	Sum of Normalized Error			χ^2 analysis (p-0.05)				Akaike Information Criteria (AIC)				Model selection criterion	
		EF	Value	RK	*df*	Calc.value	Table value	RK	$(A_{IC})_{mod}$	λ_i	*ER*	RK	Value	RK
Freundlich	2	NSD	6.3603	8	4	0.1496	9.488	8	-11.7676	0.0354	9.5843	4	2.2651	6
Langmuir	2	NSD	7.5061	18	4	0.1670	9.488	10	-7.0296	0.0033	102.4258	13	1.6383	14
Temkin	2	NSD	4.7721	2	4	0.1026	9.488	6	-12.2426	0.0448	7.5580	3	2.3683	4
D-R	2	χ^2	8.9350	19	4	0.3026	9.488	11	-2.0904	0.0003	1210.4068	15	2.0635	11
H-J	2	HYBRID	5.2870	4	4	0.3525	9.488	12	-7.4073	0.0040	84.7987	11	1.5762	17
F-H-H	2	NSD	7.1578	14	4	0.1496	9.488	8	-11.7676	0.0354	9.5843	4	2.2663	5
BET1	2	NSD	6.9096	12	4	0.1667	9.488	9	-7.0450	0.0033	101.6406	12	1.9966	13
BET 2	3	χ^2	6.8166	11	3	0.0503	7.815	2	-16.2878	0.3390	1.0000	1	3.0413	2
BET 3	3	χ^2	7.0100	13	3	0.0503	7.815	2	-16.2878	0.3390	1.0000	1	3.0448	1
Redlich-Peterson	3	EABS	5.0828	3	3	0.1009	7.815	13	-10.7609	0.0214	15.8547	7	2.1120	10
Toth	3	NSD	6.3803	9	3	0.4449	7.815	14	4.1817	1.217×10^{-5}	27855.4010	16	0.5768	19
Sips	3	NSD	6.3063	6	3	0.1296	7.815	7	0.6508	7.112×10^{-5}	4766.3842	17	0.5760	18
Khan	3	NSD	7.2572	16	3	0.0950	7.815	3	-11.0676	0.0249	13.6007	5	2.1623	8
Radke-Prausnitz	3	NSD	7.3601	17	3	0.0950	7.815	3	-11.0676	0.0249	13.6007	5	2.1624	7
Fritz-Schlüender	3	χ^2	6.3172	7	3	1.0090	7.815	4	-10.7610	0.0214	15.8537	6	2.1130	9
Fritz-Schlüender	4	NSD	7.2517	15	2	0.1020	5.991	5	-8.7610	0.0079	43.0948	9	1.8945	12
Bauder	4	NSD	6.7445	10	2	0.0340	5.991	1	-13.5762	0.0874	3.8800	2	2.6347	3
Marczewiski-Jaroniec	4	MPSD	6.2345	5	2	0.1496	5.991	8	-7.7675	0.0048	70.8233	10	1.5873	15
Fritz-Schlüender	5	NSD	4.6506	1	1	0.1604	3.841	9	-6.7246	0.0028	119.3006	14	1.5797	16

EF, RK, *df* deonte error function, ranking, degree of freedom, respectively.

Table 7. Results of SNE and criterion for kinetic models.

Kinetic models	Sum of normalized error (SNE)									χ^2 analysis (p-0.05)		
	50 mg/L			100 mg/L			150 mg/L			Average calc. value	Table value	RK
	EF	Value	RK	EF	Value	RK	EF	Value	RK			
Fractional power model	RMSE	6.3819	4	NSD	4.5572	3	NSD	3.7526	2	0.0796	21.026	4
Lagergren pseudo first-order kinetic model	NSD	4.7505	2	NSD	5.3946	4	EABS	5.0542	4	0.0632	21.026	3
Pseudo second-order model	NSD	3.9002	1	ARE	0.8418	1	NSD	1.6201	1	0.0200	21.026	1
Elovich	NSD	5.2056	3	NSD	3.0317	2	NSD	4.1980	3	0.0606	21.026	2
Avrami	HYBRID	6.7487	5	HYBRID	5.9436	5	SRE	5.06358	5	0.5376	21.026	5

Table 8. Results of Akaike information criterion (AIC) and model selection criterion for kinetic models.

Kinetic model	Akaike Information Criteria (AIC)										Model Selection Criterion			
	$(A_{IC})_{mod}$			λ_i			ER							
	50 mg/L	100 mg/L	150 mg/L	50 mg/L	100 mg/L	15 0mg/L	50 mg/L	100 mg/L	150 mg/L	RK	50 mg/L	100 mg/L	150 mg/L	RK
Fractional Power Model	-12.2731	-17.3627	-14.2193	8.88×10^{-7}	1.131×10^{-5}	4.94×10^{-5}	1126193	88391.2551	202.3735	3	-0.1795	1.4627	-0.0704	4
Lagergren pseudo first-order	-35.4483	-17.6250	-7.0307	0.0957	1.29×10^{-5}	1.36×10^{-4}	10.4516	77527.2197	7364.1813	4	4.1554	3.2983	1.6852	3
Pseudo second-order	-35.8797	-33.9844	-22.6302	0.1187	4.60×10^{-2}	3.31×10^{-1}	8.42363	21.729588	3.0182	1	4.2616	4.3762	3.7118	1
Elovich	-13.0613	-19.2412	-17.9316	1.317×10^{-6}	2.894×10^{-5}	3.16×10^{-2}	759386	34553.8386	31.6243	2	0.1019	3.9906	2.8902	2
Avrami	-4.1626	-0.8986	28.5513	1.539×10^{-8}	3.01×10^{-9}	2.55×10^{-12}	$6.5 \times 10^{+7}$	332316707	3.92×10^{11}	5	-2.5942	-3.0839	-2.2609	5

Table 9. Thermodynamic parameters for the adsorption of MB on chitosan flakes.

T (K)	ΔG^0 (kJ/mol)	ΔH^0 (kJ/mol)	ΔS^0 (kJ/(mol K))	E_a (kJ/mol)	S^* (mg/L)
313	-10077.76	4.23	0.4563	5.1575	0.0731
323	-10514.84				
343	-11339.97				
353	-11875.64				
363	-12374.26				
373	-12804.01				

in the FTIR study at wavelengths 3419.79 and 3458.21 cm^{-1} before and after adsorption of MB respectively (Bello and Olafadehan, 2021). The ionization of these functional groups is a function of the pH of MB solution that causes the surface of CH to be electrically charged. The amide and hydroxyl groups on the surface of the biosorbent can either gain or lose a proton (that is, hydrogen ion), thereby resulting in the variation of surface charge
of CH with pH of MB solution.

At low-level of pH of MB solution, protonation takes place on the active centers (that is, sites) of the chitosan flakes. Hence, the surface of the adsorbent (chitosan flakes) acquires a positive charge owing to the reactions between each of OH^- and NH_2^- functional groups on the adsorbent surface and the hydrogen ion (H^+) in solution. These reactions are represented in Equations 74 and 75, respectively:

$$CH - OH + H^+ \longrightarrow CH{-}OH_2^+ \quad (74)$$

$$CH - NH_3 + H^+ \longrightarrow CH{-}NH_4^+ \quad (75)$$

Deprotonation occurs at high pH of MB solution and the active sites on the surface of CH acquire a negative charge owing to the reactions between each of OH^- and NH_2^- functional groups on the surface of CH and the hydroxyl ion (OH^-). These reactions are represented in Equations 76 and 77, respectively:

$$CH - OH + OH^- \longrightarrow CH{-}O^- + H_2O \quad (76)$$

$$CH - NH_3 + OH^- \longrightarrow CH{-}NH_2^- + H_2O \quad (77)$$

Hence, Equations 76 and 77 reveal that electrostatic force of attraction enhances MB adsorption onto CH at high-level of MB solution pH. Thus, the reaction mechanism of MB adsorption onto the synthesized chitosan flakes from African giant snail (*A. marginata*) shell

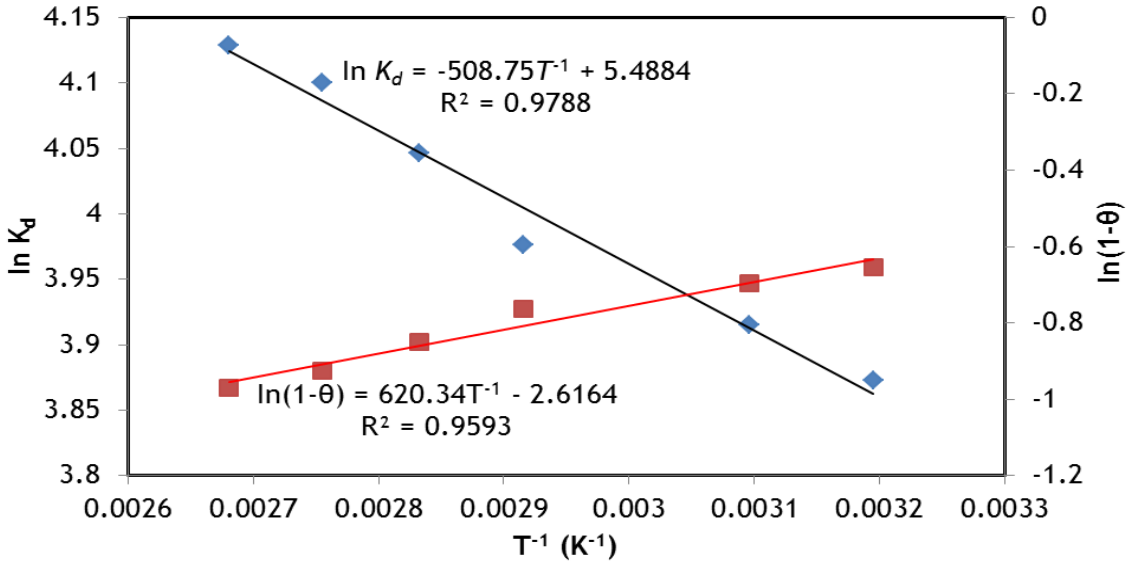

Figure 10. Variation of distribution coefficient and surface coverage with temperature.

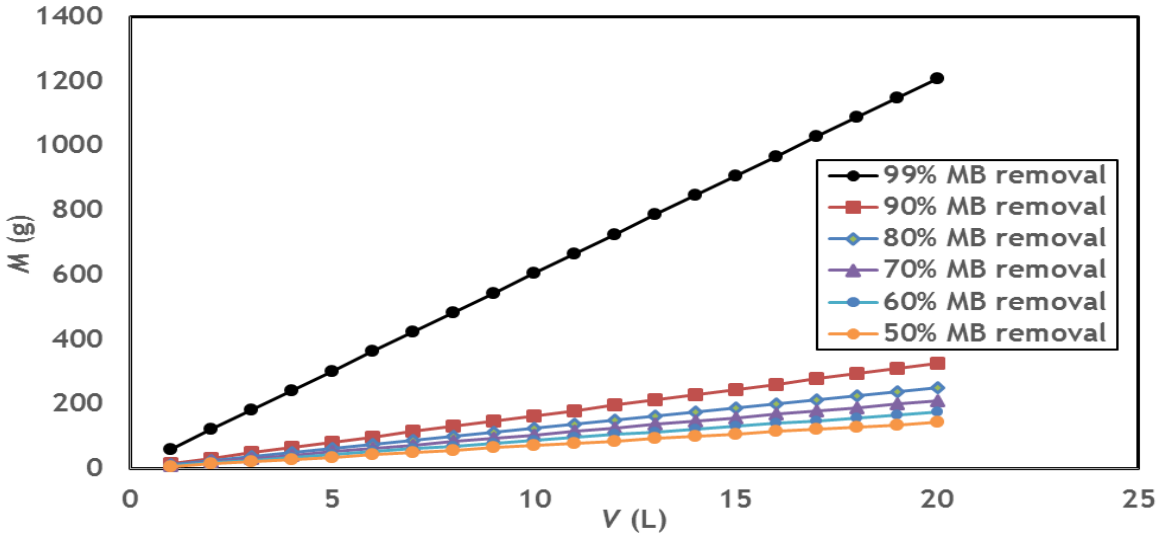

Figure 11. Variation of the theoretical mass of chitosan flakes with volume required for MB effluents to be treated for 50-99% efficiency with initial concentration of 50 mg/L at 303K.

powder is proposed thus:

$$CH - O^- + MB^+ \longrightarrow CH - O^- \cdots MB^+$$

$$CH - NH_2^- + BGD^+ \longrightarrow CH - COO^- \cdots MB^+$$

Conclusion

The capacity of chitosan extracted from African giant snail (*A. marginata*) shell powder in the removal of methylene blue (MB) from aqueous solution and the effects of operational parameters on its adsorption capacity in a batch system were investigated in this study. Equally, modeling of the adsorption equilibrium data using 19 isotherms and 8 kinetic models coupled with statistical criteria of Akaike information criteria (*AIC*), evidence ratio (*ER*), model selection criterion (*MSC*) and sum of normalized error (*SNE*) to select the best isotherm and kinetic models was carried out. The thermodynamic parameters such as activation energy, E_a, changes in enthalpy, ΔH^0, entropy, ΔS^0 and Gibbs free energy, ΔG^0, were evaluated. The most important conclusions

from this work are summarized thus:

(1) The *A. marginata* shell waste is an abundant and cheaply available precursor for the production of chitosan.
(2) The produced chitosan flake is potentially viable as an adsorbent for the removal of MB from aqueous solution. Consequently, it may be an alternative to costly biosorbents.
(3) The 5-p Fritz-Schlüender isotherm best fitted the experimental equilibrium adsorption data of MB on chitosan flakes based on the sum of normalized error (SNE) and the 3-p BET3 isotherm is the most fitted model for the adsorption of MB on the prepared chitosan flakes based on the lowest values of AIC, lowest ER value and highest value of MSC.
(4) Kinetically, the pseudo second-order model well represented the adsorption rate of MB on chitosan flakes at all initial concentrations of MB investigated in this study.
(5) The intraparticle diffusion was not found to be the rate-limiting step for the adsorption of MB on the synthesized chitosan flakes but rather film (i.e., external) diffusion and the sorption process was chemisorption-influenced.
(6) The adsorption of MB on the prepared chitosan flakes from *A. marginata* shell powder is a physical and endothermic process with ΔH^0 = 4.23 kJ/mol, a high degree of randomness at the chitosan-MB interface (ΔS^0 = 0.4563 kJ/mol), high degree of spontaneity (negative ΔG^0 values), energetically favorable and exergonic.
(7) The data reported in this study can be of beneficial use in the conception and construction of a less-costly viable treatment process using batch reactor for MB adsorption on a biosorbent and for diluting industrial effluents.

CONFLICT OF INTERESTS

The authors have not declared any conflict of interests.

REFERENCES

Adekunbi EA, Babajide JO, Oloyede HO, Amoko JS, Obijole OA, Oke IA (2019). Evaluation of Microsoft excel solver as a tool for adsorption kinetics determination. Ife Journal of Science 21(3):169-183.

Afroze S, Sen TK, Ming A, Nishioka H (2015). Adsorption of methylene blue dye from aqueous solution by novel biomass Eucalyptus sheathiana bark: equilibrium, kinetics, thermodynamics and mechanism. Desalination and Water Treatment 57(13):5858-5878.

Agarwal AK, Kadu MS, Pandhurnekar CP, Mahendra IL (2014). Langmuir, Freundlich and BET adsorption isotherm studies for zinc ions onto coal fly ash. International Journal of Application or Innovation in Engineering Management (IJAIEM) 3(1):64-71.

Ahmad MA, Puad NAA, Bello OS (2014). Kinetic, equilibrium and thermodynamic studies of synthetic dye removal using pomegranate peel activated carbon prepared by microwave-induced KOH activation. Water Resources and Industry 6:18-35.

Ahmed MJ, Hameed BH, Hummadi EH (2020). Review on recent progress in chitosan/chitin-carbonaceous material composites for the adsorption of water pollutants. Carbohydrate Polymers 116690.

Akaike H (1974). A new look at the statistical model identification. IEEE Transactions on Automatic Control 19(6):716-723.

Akpa OM, Unuabonah EI (2011). Small-sample corrected Akaike information criterion: An appropriate statistical tool for ranking of adsorption isotherm models. Desalination 272(1-3):20-26.

Alghamdi AA, Al-Odaymi ABA, Saeed WS, Al-Kahtani A, Alharthi FA, Aouak T (2019). Efficient adsorption of lead (II) from aqueous phase solutions using polypyrole-based activated carbon. Materials. Available at: https://doi.org/10.3390/ma12122020

Alston JR, Banks DJ, McNeill CX, Mitchell JB, Popov LD, Shcherbakov IN, Poler JC (2015). Adsorption studies of divalent, dinuclear coordination complexes as molecular spacers on SWCNTs. Physical Chemistry Chemical Physics 17(44):29556-29573.

Amoo KO, Olafadehan OA, Ajayi TO (2019). Optimization studies of chitin and chitosan production from penaeus notialis shell waste. African Journal of Biotechnology 18(27):670-688.

Amrhar O, Nassali H, Elyoubi MS (2015a). Two and three-parameter isothermal modeling for adsorption of crystal violet dye onto natural illitic clay: nonlinear regression analysis. Journal of Chemical and Pharmaceutical Research 7(9):892-903.

Amrhar O, Nassali H, Elyoubi MS (2015b). Application of nonlinear regression analysis to select the optimum adsorption isotherm for methylene blue adsorption onto natural illitic clay. Bulletin de la Société Royale des Sciences de Liège 84:116-130.

Anirudhan TS, Radhakrishnan PG (2009). Kinetic and equilibrium modeling of cadmium (II) ions sorption onto polymerized tamarind fruit shell. Desalination 249(3):1298-1307.

Annadurai G, Chellapandian M, Krishnan MRV (1999). Adsorption of reactive dye on chitin. Environmental Monitoring and Assessment 59(1):111-119.

Annadurai G, Krishnan MRV (1997). Batch equilibrium adsorption of reactive dye onto natural biopolymer. Iranian Polymer Journal 6(3):169-175.

Annadurai G, Ling LY, Lee J (2008). Adsorption of reactive dye from an aqueous solution by chitosan: isotherm, kinetic and thermodynamic analysis. Journal of Hazardous Materials 152(1):337-346.

Asfour HM, Fadali OA, Nassar MM, Elgeundi MS (1985a). Equilibrium studies on adsorption of basic dyes on hardwood. Journal of Chemical Technology and Biotechnology 35(1):21-27.

Asfour HM, Nassar MM, Fadali OA, Elgeundi MS (1985b). Colour removal from textile effluents using hardwood sawdust as an absorbent. Journal of Chemical Technology and Biotechnology 35(1):28-35.

Atun G, Hisarli G, Sheldrick WS, Muhler M (2003). Adsorptive removal of methylene blue from colored effluents on fuller's earth. Journal of Colloid and Interface Science 261(1):32-39.

Avrami M (1939). Kinetics of phase change. I. General theory. The Journal of Chemical Physics 7(12):1103-1112.

Avrami M (1940). Kinetics of phase change. II. Transformation-time relations for random distribution of nuclei. The Journal of Chemical Physics 8(2):212-224.

Avrami M (1941). Kinetics of phase change. III. Granulation, phase change, and microstructure. The Journal of Chemical Physics 9(2):177-184.

Ayawei N, Ebelegi AN, Wankasi D (2017). Modelling and Interpretation of Adsorption Isotherms. Journal of Chemistry 2017:1-11.

Banerjee S, Chattopadhya MC (2013). Adsorption characteristics of modified wheat husk for the removal of a toxic dye, methylene blue, from aqueous solutions. Journal of Hazardous, Toxic, and Radioactive Waste 18(1):56-63.

Behbahani TJ, Behbahani ZJ (2014). A new study on asphaltene adsorption in porous media. Petroleum and Coal 56(5):459-466.

Bello VE, Olafadehan OA (2021). Comparative investigation of RSM and ANN for multi-response modeling and optimization studies of derived chitosan from Archachatina marginata shell. Alexandria Engineering Journal 60(4):3869-3899.

Benzaoui Z, Selatnia A, Djabali D (2018). Adsorption of copper (II) ions from aqueous solution using bottom ash of expired drugs

incineration. Adsorption Science and Technology 36(1-2):114-129.
Bernal V, Erto A, Giraldo L, Moreno-Piraján J (2017). Effect of solution pH on the adsorption of paracetamol on chemically modified activated carbons. Molecules 22(7):1032. Available at: https://doi.org/10.3390/molecules22071032
Boumediene M, Benaissa H, George B, Molina S, Merlin A (2018). Effects of pH and ionic strength on methylene blue removal four synthetic aqueous by sorption onto orange peel and desorption study. Journal of Materials and Environmental Sciences 9(6):1700-1711.
Boyd G, Adamson A, Myers L (1947). The exchange adsorption of ions from aqueous solutions by organic zeolites. II. Kinetics. Journal of the American Chemical Society 69(11):2836-2844.
Castillejos E, Rodríguez-Ramos I, Soria Sánchez M, Muñoz V, Guerrero-Ruiz A (2011). Phenol adsorption from water solutions over microporous and mesoporous carbon surfaces: A real time kinetic study. Adsorption 17(3):483-488.
Celebi O, Uzum C, Shahwan T, Erten HN (2007). A radiotracer study of the adsorption behavior of aqueous Ba^{2+} ions on nanoparticles of zero-valent iron. Journal of Hazardous Materials 148(3):761-767.
Chan LS, Cheung WH, Allen SJ, McKay G (2012). Error analysis of adsorption isotherm models for acid dyes onto bamboo derived activated carbon. Chinese Journal of Chemical Engineering 20(3):535-542.
Chen H, Zhao J, Dai G, Wu J, Yan H (2010). Adsorption characteristics of Pb(II) from aqueous solution onto a natural biosorbent, fallen Cinnamomum camphora leaves. Desalination 262(1-3):174-182.
Chen Q, Tian Y, Li P, Yan C, Pang Y, Zheng L, Meng X (2017). Study on shale adsorption equation based on monolayer adsorption, multilayer adsorption, and capillary condensation. Journal of Chemistry Article ID 1496463:1-11.
da Silva Alves DC, Healy B, de Almeida Pinto LA, Cadaval Jr TRSA, Breslin CB (2021). Recent developments in chitosan-based adsorbents for the removal of pollutants from aqueous environments, Molecules 26(3):594. Available at: https://doi.org/10.3390/molecules26030594
Dávila-Jiménez MM, Elizalde-González MP, García-Díaz E, González-Perea M, Guevara-Villa MRG (2014). Using Akaike information criterion to select the optimal isotherm equation for adsorption from solution. Adsorption Science and Technology 32(7):605-622.
Deng S, Chen Y (2019). A study by response surface methodology (RSM) on optimization of phosphorus adsorption with nano spherical calcium carbonate derived from waste. Water Science and Technology 79(1):188-197.
Derakhshan Z, Baghapour MA, Ranjbar M, Faramarzian M (2013). Adsorption of methylene blue dye from aqueous solutions by modified pumice stone: kinetics and equilibrium studies. Health Scope 2(3):136-144.
Dil EA, Ghaedi M, Asfaram A, Mehrabi F, Bazrafshan AA, Ghaedi AM (2016). Trace determination of safranin O dye using ultrasound assisted dispersive solid phase micro extraction: artificial neural network-genetic algorithm and response surface methodology. Ultrasonics Sonochemistry 33:129-140.
Dubinin MM (1960). The potential theory of adsorption of gases and vapours for adsorbents with energetically nonuniform surfaces. Chemical Reviews 60(2):235-241.
Ebadi A, Soltan Mohammadzadeh JS, Khudiev A (2009). What is the correct form of BET isotherm for modeling liquid phase adsorption? Adsorption 15(1):65-73.
Edet UA, Ifelebuegu OA (2020). Kinetics, isotherm, and thermodynamics modeling of the adsorption of phosphates from model wastewater using recycled brick waste. Processes 8(665):1-15.
El-Geundi MS (1991). Colour removal from textile effluents by adsorption techniques. Water Research 25(3):271-273.
Elizalde-González MP, Hernández-Montoya V (2009). Removal of acid orange 7 by guava seed carbon: A four parameter optimization study. Journal of Hazardous Materials 168(1):515-522.
El-Khaiary MI, Malash GF (2011). Common data analysis errors in batch adsorption studies. Hydrometallurgy 105(3-4):314-320.
Elmorsi MT (2011). Equilibrium isotherms and kinetic studies of removal of methylene blue dye by adsorption onto miswak leaves as a natural adsorbent. Journal of Environmental Protection 2(6):817-827.
Erdem E, Karapinar N, Donat R (2004). The removal of heavy metal cations by natural zeolites. Journal of Colloid and Interface Science 261(2):309-319.
Fan L, Luo C, Sun M, Qiu H, Li X (2013). Synthesis of magnetic β-cyclodextrin–chitosan/graphene oxide as nanoadsorbent and its application in dye adsorption and removal. Colloids and Surf B: Biointerf 103:601-607.
Fan L, Luo CN, Sun M, Li XJ (2012). Fabrication of magnetic chitosan nanoparticles grafted with β-cyclodextrin as effective adsorbents toward hydroquinol. Colloids and Surfaces B: Biointerfaces 95:42-49.
Freundlich HMF (1906). Uber die Adsorption in Losungen. Zeitschrift für Physikalische Chemie 57(1):385-470.
Ghaedi M, Hajjati S, Mahmudi Z, Tyagi I, Agarwal S, Maity A, Gupta VK (2015). Modeling of competitive ultrasonic assisted removal of the dyes – methylene blue and safranin-O using Fe_3O_4 nanoparticles. Chemical Engineering Journal 268:28-37.
Ghaffari HR, Pasalari H, Tajvar A, Dindarloo K, Goudarzi B, Alipour V, Ghanbarneajd A (2017). Linear and non linear two-parameter adsorption isotherm modelling: A case study. The International Journal of Engineering and Science 6(9):1-11.
Ghogomu JN, Noufame TD, Ketcha MJ, Ndi NJ (2013). Removal of Pb (II) ions from aqueous solutions by kaolinite and metakaolinite materials. British Journal of Applied Science and Technology 3(4):942-961.
Gunay A, Arslankaya E, Tosun I (2007). Lead removal from aqueous solution by natural and pretreated clinoptilolite: adsorption equilibrium and kinetics. Journal of Hazardous Materials 146(1-2):362-371.
Gupta S, Kumar A (2019). Removal of nickel (II) from aqueous solution by biosorption on A. Barbadensis miller waste leaves powder. Applied Water Science 9(96):1-11.
Gupta VK, Jain KR, Nayak A, Agarwal S, Shrivastava M (2011). Removal of the hazardous dye – Tartrazine by photodegradation on titanium dioxide surface. Materials Science and Engineering: C 31(5):1062-1067.
Gupta VK, Suhas, Tyagi I, Agarwal S, Singh R, Chaudhary M, Harit A, Kushwaha S (2016). Column operation studies for the removal of dyes and phenols using a low cost adsorbent. Global Journal of Environmental Science and Management 2(1):1-10.
Hall KR, Eagleton LC, Acrivos A, Vermeulen T (1966). Pore- and solid-diffusion kinetics in fixed-bed adsorption under constant-pattern conditions. Industrial and Engineering Chemistry Fundamentals 5(2):212-223.
Hamdaoui O (2006). Batch study of liquid-phase adsorption of methylene blue using cedar sawdust and crushed brick. Journal of Hazardous Materials B 135(1-3):264-273.
Hamdaoui O, Naffrechoux E (2007). Modeling of adsorption isotherms of phenol and chlorophenols onto granular activated carbon Part I. Two-parameter models and equations allowing determination of thermodynamic parameters. Journal of Hazardous Materials 147(1-2):381-394.
Hamed I, Özogu F, Regenstein JM (2016). Industrial applications of crustacean by-products (chitin, chitosan, and chitooligosaccharides): A review. Trends in Food Science and Technology 48:40-50.
Hameed BH, Ahmad AL (2009). Batch adsorption of methylene blue from aqueous solution by garlic peel, an agricultural waste biomass. Journal of Hazardous Materials 164(2-3):870-875.
Hameed BH, Din ATM, Ahmad AL (2007). Adsorption of methylene blue onto bamboo-based activated carbon: Kinetics and equilibrium studies. Journal of Hazardous Materials 141(3):819-825.
Hasan MB (2008). Adsorption of reactive azo dyes on chitosan/oil-palm ash composite adsorbent: batch and continuous studies. M. Sc. Thesis, Universiti Sains Malaysia.
He J, Hong S, Zhang L, Gan F, Ho YS (2010). Equilibrium and thermodynamics parameters of adsorption of methylene blue onto rectorite. Fresenius Environmental Bulletin 19(11a):2651-2656.
Hefni HHH, Nagy M, Azab MM, Hussein MHM (2019). O-acylation of chitosan by L-arginine to remove the heavy metals and total organic carbon (TOC) from wastewater. Egyptian Journal of Petroleum 29(1):31-38.
Ho YS (2004). Comments on an evaluation of copper biosorption by a brown seaweed under optimized conditions by Antunes W. M., Luna, A. S., Henriques. C. A. and da Costa, A. C. A. Electronic Journal of

Biotechnology 7(2):228-237.
Ho YS, Porter JF, Mckay G (2002). Equilibrium isotherm studies for the biosorption of divalent metal ions onto peat, copper, nickel and lead single component systems. Water, Air, and Soil Pollution 141(1):1-33.
Hong S, Wen C, He J, Gan FX, Ho YS (2009). Adsorption thermodynamics of methylene blue onto bentonite. Journal of Hazardous Materials 167(1-3):630-633.
Horsfall Jnr M, Spiff A (2005). Effects of temperature on the sorption of Pb^{2+} and Cd^{2+} from aqueous solution by Caladium bicolor (wild Cocoyam) biomass. Electronic Journal of Biotechnology 8(2):162-169.
Hu ZG, Zhang J, Chan WL, Szeto YS (2006). The sorption of acid dye onto chitosan nanoparticles. Polymer 47(16):5838-5842.
Húmpola PD, Odetti HS, Fertitta AE, Vicente JL (2013). Thermodynamic analysis of adsorption models of phenol in liquid phase on different activated carbons. Journal of the Chilean Chemical Society 58(1):1541-1544.
Hurvich CF, Tsai CL (1989). Regression and time series model selection in small samples. Biometrika 76(2):297-307.
Ibrahim HA, Abdel Moamen OA, Monem NA, Ismail IM (2018). Assessment of kinetic and isotherm models for competitive sorption of Cs^{+} and Sr^{2+} from binary metal solution onto nanosized zeolite. Chemical Engineering Communication 205(9):1274-1287.
Inam E, Etim UJ, Akpabio EG, Umoren SA (2016). Process optimization for the application of carbon from plantain peels in dye abstraction. Journal of Taibah University for Science 11(1):173-185.
Israel U, Eduok UM (2012). Biosorption of zinc from aqueous solution using coconut (*Cocos nucifera* L) coirdust. Archives of Applied Science Research 4(2):809-819.
Khodaie M, Ghasemi N, Moradi B, Rahim M (2013). Removal of methylene blue from wastewater by adsorption onto $ZnCl_2$ activated corn husk carbon equilibrium studies. Journal of Chemistry. Available at: http://dx.doi.org/10.1155/2013/383985
Kolmogorov A, Petrovskii I, Piskunov N (1937). A study of the diffusion equation with increase in the amount of substance, and its application to a biological problem. Bulletin of Moscow University Mathematics and Mechanics 1(6):1-26.
Kuang Y, Zhang X, Zhou S (2020). Adsorption of methylene blue in water onto activated carbon by surfactant modification. Water 12(2):587. Available at: https://doi.org/10.3390/w12020587
Kumar ASK, Ramachandran R, Kalidhasan S, Rajesh V, Rajesh N (2012). Potential application of dodecylamine modified sodium montmorillonite as an effective adsorbent for hexavalent chromium. Chemical Engineering Journal 211:396-405.
Kyzas GZ, Christodoulou E, Bikiaris DN (2018). Basic dye removal with sorption onto low-cost natural textile fibers. Processes 6(9):166. Available at: https://doi.org/10.3390/pr6090166
Langmuir I (1918). The adsorption of gases on plane surfaces of glass, mica and platinum. Journal of the American Chemical Society 40(9):1361-1403.
Li Y, Sun J, Du Q, Zhang L, Yang X, Wu S, Xia Y, Wang Z, Xia L, Cao A (2014). Mechanical and dye adsorption properties of graphene oxide/chitosan composite fibers prepared by wet spinning. Carbohydrate Polymers 102:755-761.
Magdy YM, Altaher H, ElQada E (2018). Removal of three nitrophenols from aqueous solutions by adsorption onto char ash: equilibrium and kinetic modeling. Applied Water Science 8(1):1-15. Available at: https://doi.org/10.1007/s13201-018-0666-1
Mahmoud ME, Nabil GM, El-Mallah NM, Bassiouny HI, Kumar S, Abdel-Fattah TM (2016). Kinetics, isotherm, and thermodynamic studies of the adsorption of reactive red 195 A dye from water by modified switchgrass biochar adsorbent. Journal of Industrial and Engineering Chemistry 37:156-167.
Malash GF, El-Khaiary MI (2010). Piecewise linear regression: A statistical method for the analysis of experimental adsorption data by the intraparticle-diffusion models. Chemical Engineering Journal 163(3):256-263.
Malik PK (2004). Dye removal from wastewater using activated carbon developed from sawdust: adsorption equilibrium and kinetics. Journal of Hazardous Materials 113(1-3):81-88.
Marshall WE, Champagne ET (1995). Agricultural byproducts as adsorbents for metal ions in laboratory prepared solutions and in manufacturing wastewater. Journal of Environmental Science & Health Part A 30(2):241-261.
Marshall WE, Johns MM (1996). Agricultural by-products as metal adsorbents: Sorption properties and resistance to mechanical abrasion. Journal of Chemical Technology and Biotechnology 66(2):192-198.
McKay G, Elgeundi M, Nassar MM (1987). Equilibrium studies during the removal of dyestuffs from aqueous solutions using bagasse pith. Water Research 21(12):1513-1520.
Mitrevski V, Mitrevski C, Mijakovski V, Pavkov IS, Geramitcioski T (2017). Mathematical modelling of the sorption isotherms of Quince. Thermal Science 21(5):1965-1973.
Mittal A, Mittal J, Malviya A, Gupta VK (2010). Removal and recovery of Chrysoidine Y from aqueous solutions by waste materials. Journal of Colloid and Interface Science 344(2):497-507.
Mohan D, Singh KP (2002). Single- and multi-component adsorption of cadmium and zinc using activated carbon derived from bagasse – An agricultural waste. Water Research 36(9):2304-2315.
Morrison RT, Boyd RN (2004). Organic Chemistry, Pearson Education, Singapore.
Muxika A, Etxabide A, Uranga J, Guerrero P, de la Caba K (2017). Chitosan as a bioactive polymer: processing, properties and applications. International Journal of Biological Macromolecules 105(2):1358-1368.
Najim TS, Yassin SA, Majli AJ (2010). Poly (furfural-acetone) as new adsorbent for removal of Cu (II) from aqueous solution: Thermodynamics and kinetic studies. International Journal of Chemistry 2(2):44-53.
Namasivayam C, Arasi D (1997). Removal of Congo red from wastewater by adsorption onto waste red mud. Chemosphere 34(2):401-417.
Namasivayam C, Kavitha D (2002). Removal of Congo red from water by adsorption onto activated carbon prepared from coir pith, an agricultural solid waste. Dyes and Pigments 54(1):47-58.
Namasivayam C, Radhika R, Suba S (2001a). Uptake of dyes by a promising locally available agricultural solid waste: coir pith. Waste Management 21(4):381-387.
Namasivayam C, Yamuna RT, Arasi D (2001b). Removal of acid violet from wastewater by adsorption on waste red mud. Environmental Geology 41(3):269-273.
Namasivayam C, Yamuna RT, Arasi D (2002). Removal of procion orange from wastewater by adsorption on waste red mud. Separation Science and Technology 37(10):2421-2431.
Nayak AK, Pal A (2019). Development and validation of an adsorption kinetic model at solid-liquid interface using normalized Gudermannian function. Journal of Molecular Liquids 276:67-77.
Nekouei F, Nekouei S, Tyagi I, Gupta VK (2015). Kinetic, thermodynamic and isotherm studies for acid blue 129 removal from liquids using copper oxide nanoparticle-modified activated carbon as a novel adsorbent. Journal of Molecular Liquids 201:124-133.
Olafadehan OA (2021). Fundamentals of Adsorption Processes, ISBN: 978-620-3-30705-4, LAP Lambert Academic Publishing, OmniScriptum DUE GmbH.
Olafadehan OA, Ajayi TO, Amoo KO (2020). Optimum conditions for extraction of chitin and chitosan from callinectes amnicola shell waste. Theoretical Foundations of Chemical Engineering 54(6):1173-1194.
Olafadehan OA, Akpo OY, Enemuo O, Amoo KO, Abatan OG (2018). Equilibrium, kinetic and thermodynamic studies of biosorption of zinc ions from industrial wastewater using derived composite biosorbents from walnut shell. African Journal of Environmental Science and Technology 12(9):335-356.
Olafadehan OA, Amoo KO, Ajayi TO, Bello VE (2021). Extraction and characterization of chitin and chitosan from Callinectes amnicola and Penaeus notialis shell wastes. Journal of Chemical Engineering and Material Science 12(1):1-30.
Padder MS, Majumder CB (2016). Studies on removal of As(III)and As(V) through their adsorption onto granular activated carbon/$MnFe_2O_4$ composite: isotherm studies and error analysis. Composite Interface 23(4):327-372.
Padmesh TVN, Vijayaraghavan K, Sekaran G, Velan M (2006). Application of two-and three-parameter isotherm models: b iosorption

of acid red 88 onto Azolla microphylla. Bioremediation Journal 10(1-2):37-44.
Pandey S, Mishra SB (2011). Organic–inorganic hybrid of chitosan/organoclay bionanocomposites for hexavalent chromium uptake. Journal of Colloid and Interface Science 361(2):509-520.
Periolatto M, Ferrero F (2013). Cotton Filter Fabrics Functionalization by Chitosan UV grafting for Removal of Dyes. Chemical Engineering Transactions 32:85-90.
Poots VJP, McKay G, Healy JJ (1976). The removal of acid dye from effluent using natural adsorbents—I peat. Water Research 10(12):1061-1066.
Popoola LT (2019). Characterization and adsorptive behavior of snail shell-rice husk (SS-RH) calcined particles (CPs) towards cationic dye. Heliyon 5(1):1-38.
Pourali P, Behzad M, Arfaeinia H, Ahmadfazeli A, Afshin S, Poureshgh Y, Rashtbari Y (2020). Removal of acid blue 113 from aqueous solutions using low cost adsorbent adsorption isotherms, thermodynamics, kinetics and regeneration studies. Separation Science and Technology. Available at: https://doi.org/10.1080/01496395.2020.1867583
Rahman MM, Pal A, Uddin K, Thu K, Saha BB (2018). Statistical analysis of optimized isotherm model for maxsorb III/ethanol and silical gel/water pairs. Evergreen Joint Journal of Novel Carbon Resources Sciences and Green Asia Strategy 5(4):1-12.
Rahmi HF, Susilawati, Ismaturrahmi, Nilawati (2018). Preparation of sulfonated magnetic chitosan for methylene blue adsorption. International Proceeding ASEAN YOUTH Conference, PPI-Malaysia 1:379-384.
Ramadoss R, Subramaniam D (2018). Adsorption of chromium using blue green algae-modeling and application of various isotherms. International Journal of Chemical Technology 10(1):1-22.
Razavi Z, Mirghaffari N, Rezaei B (2013). Adsorption of crude and engine oils from water using raw rice husk. Water Science and Technology 69(5):947-952.
Redlich O, Peterson DL (1959). A useful adsorption isotherm. Journal of physical chemistry 63(6):1024-1024. Available at: http://dx.doi.org/10.1021/j150576a611
Reichenberg D (1953). Properties of ion-exchange resins in relation to their structure. III. Kinetics of exchange. Journal of the American Chemical Society 75(3):589-597.
Sabar S, Aziz HA, Yusof NH, Subramaniam S, Foo KY, Wilson LD, Lee HK (2020). Preparation of sulfonated chitosan for enhanced adsorption of methylene blue from aqueous solution. Reactive and Functional Polymers 151:104584. Available at: http://dx.doi.org/10.1016/j.reactfunctpolym.2020.104584
Saha P, Chowdhury S (2011). Insight into adsorption thermodynamics. Thermodynamics 16:349-364. Available at: https://doi.org/10.5772/13474
Saleh TA, Gupta VK (2014). Processing methods, characteristics and adsorption behavior of tire derived carbons: A review. Advances in Colloid and Interface Science 211:93-101.
Salimi A, Roosta A (2019). Experimental solubility and thermodynamic aspects of methylene blue in different solvents. Thermochimica Acta 675:134-139.
Saravanam E, Khan MM, Gracia F, Qin J, Gupta VK, Stephen A (2016). Ce^{3+}-ion-induced visible-light photocatalytic degradation and electrochemical activity of ZnO/CeO_2 nanocomposite, Scientific Reports 6(1):1-11. Available at: https://doi.org/10.1038/srep31641
Saravanan R, Gupta VK, Thanigainathan P, Narayanan V, Arumainathan S (2013a). Synthesis, characterization and photocatalytic activity of novel Hg doped ZnO nanorods prepared by thermal decomposition method. Journal of Molecular Liquids 178:88-93.
Saravanan R, Joicy S, Gupta VK, Narayanan V, Stephen A (2013c). Visible light induced degradation of methylene blue using CeO_2/V_2O_5 and CeO_2/CuO catalysts. Materials Science and Engineering: C 33(8):4725-4731.
Saravanan R, Karthikeyan S, Gupta VK, Sekaran G, Narayanan V, Stephen A (2013b) Enhanced photocatalytic activity of ZnO/CuO nanocomposite for the degradation of textile dye on visible light illumination. Materials Science and Engineering: C 33(1):91-98.
Saravanan R, Karthikeyan N, Gupta VK, Thirumal E, Thangadurai P, Narayanan V, Stephen A (2013d). ZnO/Ag nanocomposite: An efficient catalyst for degradation studies of textile effluents under visible light. Materials Science & Engineering: C 33(4):2235-2244.
Saravanan R, Khan MM, Gupta VK, Mosquera E, Gracia F, Narayanan V, Stephen A (2015). ZnO/Ag/CdO nanocomposite for visible light-induced photocatalytic degradation of industrial textile effluents. Journal of Colloid and Interface Science 452:126-133.
Sarode S, Upadhyay P, Khosa MA, Mak T, Shakir A, Song S, Ullaha A (2019). Overview of wastewater treatment methods with special focus on biopolymer chitin-chitosan. International Journal of Biological Macromolecules 121:1086-1100.
Senthilkumaar S, Varadarajan PR, Porkodi K, Subbhuraam CV (2005). Adsorption fiber carbon: kinetics and equilibrium of methylene blue onto jute fiber carbon: kinetics and equilibrium studies. Journal of Colloid and Interface Science 284(1):78-82.
Shajahan A, Shankar S, Sathiyaseelan A, Narayan KS, Narayanan V, Kaviyarasan V, Ignacimuthu S (2017). Comparative studies of chitosan and its nanoparticles for the adsorption efficiency of various dyes. International Journal of Biological Macromolecules 104:1449-1458.
Sharififard H, Shahraki ZH, Rezvanpanah E, Rad SH (2018). A novel natural chitosan/activated carbon/iron bio-nanocomposite: sonochemical synthesis, characterization, and application for cadmium removal in batch and continuous adsorption process. Bioresource Technology 270:562-569.
Sharma P, Das MR (2012). Removal of a cationic dye from aqueous solution using graphene oxide nanosheets: investigation of adsorption parameters. Journal of Chemical & Engineering Data 58(1):151-158.
Sheshmani S, Ashori A, Hasanzadeh S (2014). Removal of acid orange 7 from aqueous solution using magnetic graphene/chitosan: A promising nano-adsorbent. International Journal of Biological Macromolecules 68:218-224.
Sivarajasekar N, Baskar R (2014). Adsorption of basic red onto activated carbon derived from immature cotton seeds: isotherm studies and error analysis. Desalination and Water Treatment 52(40-42):7743-7765.
Slimani R, Anouzla A, Abrouki Y, Ramli Y, Antri SE, Mamouni R, Lazar S, Haddad ME (2011). Removal of a cationic dye-methylene blue from aqueous media by the use of animal bone meal as a new low cost adsorbent. Journal of Materials and Environmental Science 2(1):77-87.
Sugiura N (1978). Further analysis of data by Akaike's information criterion and the finite corrections. Communications in Statistics – Theory and Methods A7(1):12-26.
Sun L, Tian C, Wang L, Zou JL, Mu G, Fu HG (2011). Magnetically separable porous graphitic carbon with large surface area as excellent adsorbents for metal ions and dye. Journal of Materials Chemistry 21(20):7232-7239.
Sutherland C, Venkobachar C (2010). A diffusion-chemisorption kinetic model for simulating biosorption using forest macro-fungus, fomes fasciatus. International Research Journal of Plant Science 1(4):107-117.
Tahir SS, Rauf N (2006). Removal of a cationic dye from aqueous solutions by adsorption onto bentonite clay. Chemosphere 63(11):1842-1848.
Temkin M, Pyzhev V (1940). Kinetics of ammonia synthesis on promoted iron catalyst. Acta Physiochimica 12:327-356.
Tóth J (1971). State equation of the solid gas interface layer. Acta Chimica (Academiae Scientiarum) Hungaricae 69:311-317.
Tran VS, Ngo HH, Guo W, Zhang J, Liang S, Ton-That C, Zhang X (2015). Typical low cost biosorbents for adsorptive removal of specific organic pollutants from water. Bioresource Technology 182:353-363.
Turner BD, Henley BJ, Sleap SB, Sloan SW (2015). Kinetic model selection and the Hill model in geochemistry. International Journal of Environmental Science and Technology 12:2545-2558.
Vakili M, Rafatullah M, Salamatinia B, Abdullah AZ, Ibrahim MH, Tan KB, Gholami Z, Amouzgar P (2014). Application of chitosan and its derivatives as adsorbents for dye removal from water and wastewater: A review. Carbohydrate Polymers 113:115-130.
Vandevivere PC, Bianchi R, Verstraete W (1998). Treatment and reuse

of wastewater from the textile wet-processing industry: Review of emerging technologies. Journal of Chemical Technology and Biotechnology 72(4):289-302.
Vijayaraghavan K, Padmesh TVN, Palanivelu K, Manickam V (2006). Biosorption of Nickel(II) Ions onto Sargassum wightii: Application of two-parameter and three-parameter isotherm models. Journal of Hazardous Materials 133(1-3):304-308.
Wagenmakers E, Farrell S (2004). AIC model selection using Akaike weights**.** Psychonomic Bulletin Review 11(1):192-196.
Walker GM, Weatherley LR (1997). Adsorption of acid dyes on to granular activated carbon in fixed beds. Water Research 31(8):2093-2101.
Wan Ngaha WS, Teonga LC, Hanafiaha MAKM (2011). Adsorption of dyes and heavy metal ions by chitosan composites: A review. Carbohydrate Polymers 83(4):1446-1456.
Wang QL, Apul OG, Xuan P, Luo F, Karanfil T (2013). Development of a 3DQSPR model for adsorption of aromatic compounds by carbon nanotubes: comparison of multiple linear regression, artificial neural network and support vector machine. RSC Advances 3(46):1-32.
Wang S, Li L, Wu H, Zhu ZH (2005). Unburned carbon as a low-cost adsorbent for treatment of methylene blue-containing wastewater. Journal of Colloid and Interface Science 292(2):336-343.
Wang XS, Qin Y, Li ZF (2006). Biosorption of zinc from aqueous solutions by rice bran: kinetics and equilibrium studies, Separation Science and Technology 41(4):747-756.
Weber TW, Chakravorti RK (1974). Pore and solid diffusion models for fixed-bed adsorbers. AIChE Journal 20(2):228-238.
Yanev ZL, Koumanova BK, Georgieva NV (2013). Linear and nonlinear regression methods for equilibrium modelling of p-nitrophenol biosorption by Rhizopus Oryza: comparison of error analysis criteria. Journal of Chemistry 2013:1-10.
Yao YJ, Xu FF, Chen M, Xu ZX, Zhu ZW (2010). Adsorption behavior of methylene blue on carbon nanotubes. Bioresource Technology 101(9):3040-3046.
Yoro KO, Singo M, Mulopo JL, Daramola MO (2017). Modelling and experimental study of the CO_2 capture. Energy Procedia 114:1643-1664.
Zarrouk AH, Zarrok B, Al-Salem, Sultan H, Messali M (2011). Temperature effect, activation energies and thermodynamic adsorption studies of l-cysteine methyl ester hydrochloride as copper corrosion inhibitor in nitric acid 2M. International Journal of Electrochemical Science 6(12):6261-6274.
Zbair M, Anfar Z, Khallok H, Ahsaine HA, Ezahri M, Elalem N (2018). Adsorption kinetics and surface modeling of aqueous methylene blue onto activated carbonaceous wood sawdust. Fullerenes, Nanotubes and Carbon Nanostructures 26(7):433-442.
Zhai Y, Wei X, Zeng G, Zhang D, Chu K (2004). Study of adsorbent derived from sewage sludge for the removal of Cd^{2+}, Ni^{2+} in aqueous solutions. Separation and Purification Technology 38(2):191-196.